Precambrian Research 220–221 (2012) 9–22

Contents lists available at SciVerse ScienceDirect

Precambrian Research

journal homepage: www.elsevier.com/locate/precamres

Grenville-age orogenesis in the Qaidam-Qilian block: The link between South China and Tarim

Shuguang Song[a,*], Li Su[b], Xian-hua Li[c], Yaoling Niu[d,e], Lifei Zhang[a]

[a] MOE Key Laboratory of Orogenic Belts and Crustal Evolution, School of Earth and Space Sciences, Peking University, Beijing 100871, China
[b] Laboratory Centre of Science Research Institute, China University of Geosciences, Beijing 100083, China
[c] State Key Laboratory of Lithospheric Evolution, Institute of Geology and Geophysics, Chinese Academy of Sciences, Beijing 100029, China
[d] School of Earth Sciences, Lanzhou University, Lanzhou 730000, China
[e] Department of Earth Sciences, Durham University, Durham DH1 3LE, UK

ARTICLE INFO

Article history:
Received 4 January 2012
Received in revised form 17 July 2012
Accepted 21 July 2012
Available online xxx

Keywords:
North Qaidam UHPM belt
Grenville-age
Orogeny
Geochronology
South-West China United Continent

ABSTRACT

The link between the South China and Tarim blocks is a key issue in defining the tectonic framework of China. We report here that rocks from the Paleozoic (Caledonian) ultrahigh-pressure metamorphic (UHPM) belt also record a Grenville-age orogenic event in the Qaidam-Qilian block that lies between the South China and Tarim blocks. This event is marked by the presence of a juvenile Grenville-age continental margin that had been subducted to and exhumed from mantle depths of 100–200 km at the present-day location of northern Tibetan Plateau. The magmatic and metamorphic ages of 900–1000 Ma recorded in the gneisses provide direct evidence for this Grenville-age orogeny that extends northwestward from the Yangtze block, to the Qaidam-Qilian block, and to the Tarim block. This Grenville-age orogen along the North Qaidam UHPM belt (1) represents the link for the once South China–Qaidam-Qilian–Tarim continent, which, we name here as the "South-West China United Continent (SWCUC)", had existed before the India–Asia collision, (2) sets a framework for precise reconstruction of Supercontinent Rodinia, and (3) presents an example of multi-epoch tectonic recycles, represented by the Neoproterozoic Grenvillian orogenesis and the Early Paleozoic Caledonian orogenesis.

1. Introduction

Three major tectonic blocks define the tectonic framework of the continental China; this includes the North China Craton (NCC), the South China Craton (Yangtze and Cathaysia blocks as SCC) and the Tarim Craton (Fig. 1a). It is well known that the NCC and SCC have independent evolution histories from the Neoproterozoic to Paleozoic before their final collision along the Dabie-Sulu UHPM belt in the Triassic (e.g., Li et al., 1993; Hacker et al., 1998).

The triangle-shaped NCC is believed to have formed by collision of two Archean nuclei along the central belt at ~1.8–1.9 Ga (e.g., Zhao et al., 2005). The SCC, on the other hand, was thought to have formed through the amalgamation of the Yangtze and Cathaysia blocks during the ca. 1.1–0.9 Ga Sibao orogenesis (e.g., Z.-X. Li et al., 2002, 2008; X.-H. Li et al., 2006, 2009a; Ye et al., 2007). The large scale of magmatic activities in the SCC over the Meso- and Neoproterozoic eras, an important time period in the Rodinia supercontinent from its amalgamation to fragmentation (e.g., Li et al., 2008 and references therein), are absent in the NCC.

The Tarim Craton is a parallelogram-shaped basin covered by a thick succession of Paleozoic to Mesozoic strata with a Precambrian basement interpreted to be a fragment of the Rodinian Supercontinent (C.-L. Zhang et al., 2007; Xu et al., 2005, 2009; Lu et al., 2008). The Permian (~290–270 Ma) continental flood basalts (CFBs) distribute as layers within much of the basin (e.g., Tian et al., 2010). Although the affinity between the Yangtze and Tarim cratons has been recognized in terms of the Neoproterozoic magmatic activity, there is a spatially large gap between the two because of the northward protrusion of the Northern Tibetan Plateau.

The India–Asia continental collision in the early Cenozoic and the continued northward convergence of the Indian Plate has obscured the tectonic framework of the continental China. The northward convergence is bounded to the west by the sinistral strike-slip Altyn Tagh Fault (Fig. 1a). The east bound is, however, rather diffusive, and is interpreted to be eastward extrusion of the continent along a series of dextral strike-slip faults (e.g., Tapponnier et al., 2001; Replumaz and Tapponnier, 2003). The Qaidam-Qilian block in the northern Tibetan Plateau is located between the SCC and Tarim Craton and has been suggested to be of Yangtze

* Corresponding author.
E-mail address: sgsong@pku.edu.cn (S. Song).

0301-9268/$ – see front matter © 2012 Elsevier B.V. All rights reserved.
http://dx.doi.org/10.1016/j.precamres.2012.07.007

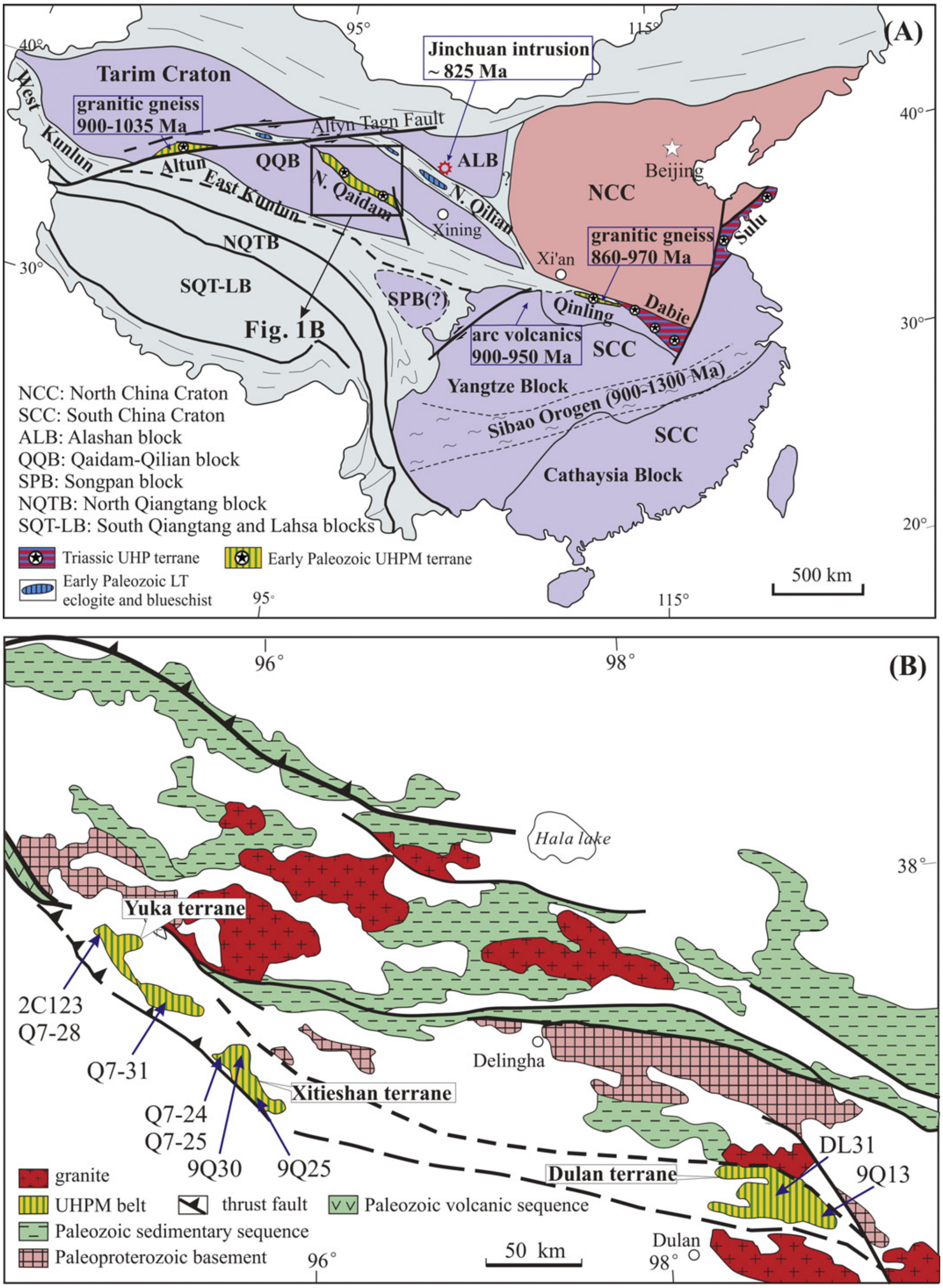

Fig. 1. (a) Tectonic framework of China showing distribution of major blocks or cratons. (b) Geological map of the North Qaidam UHPM belt with sampling localities.

affinity on the basis of Meso- to Neoproterozoic intrusions (e.g., Guo et al., 1999; Wan et al., 2001, 2006; Lu, 2002; Lu et al., 2006, 2008; Song et al., 2006; J.X. Zhang et al., 2006, 2008; C. Zhang et al., 2012; Tung et al., 2007a,b, 2012). In this paper, we report a Grenville-age orogenic belt with 1002–907 Ma magmatism and ~950–910 Ma metamorphism. Rocks of this orogenic belt had undergone subsequent ultrahigh-pressure (UHP) metamorphism during continental subduction and exhumation in the Paleozoic (~460–400 Ma). On the basis of the Grenville-age magmatism and metamorphism, we discuss the relationship among cratons/blocks of the South China, the Qaidam-Qilian, and the Tarim and reconstruction of a giant continent from southeast to northwest China.

2. Tectonic setting of the Qaidam-Qilian block

The Qilian-Qaidam mountain-basin system is located in the northern part of the Tibetan Plateau. It is also located tectonically in the central region among three major blocks, e.g., the NCC, the SCC and the Tarim Craton (Fig. 1a). This mountain-basin system includes two blocks with 1.8–2.4 Ga Paleoproterozoic basement; they are, from north to south, the Qilian block and the Qaidam block (Zhang et al., 2001a; Lu, 2002; N.S. Chen et al., 2007; N. Chen et al., 2009; Lu et al., 2006, 2008; Wang et al., 2009). Some individual granitic intrusions with ages of 880–940 Ma have been reported in the Qilian block (Guo et al., 1999; Wan et al., 2001, 2006; Lu, 2002; Xu et al., 2007; Tung et al., 2007a). The ~850 Ma CFBs, which occur as protoliths of eclogites in the North Qaidam UHPM belt (see below), have been demonstrated to be of mantle plume origin and onset of the presumed long-lived Neoproterozoic superplume that broke up the supercontinent Rodinia (Song et al., 2010a,b).

The Alashan block in the north is generally thought as the western part of the North China Craton (e.g., Zhao et al., 2005). It consists predominantly of early Precambrian basement with 2.3–1.9 Ga granitic gneiss (Xiu et al., 2004). The Archean basement is signified by the ~2.7 Ga amphibolite in the northeast part of the block (Geng et al., 2006), as well as by some 2.5–3.5 Ga detrital zircons from meta-sedimentary sequences (e.g., Geng et al., 2007; Tung et al., 2007a). Recent studies by Dan et al. (2012) indicate that the primary magmatic ages of the mafic and felsic igneous rocks are ca. 2.34–2.30 Ga with zircon Hf model ages of 2.92–2.81 Ga. 845–971 Ma foliated granite intrusions were recognized (Wan et al., 2001). A ~825 Ma Cu–Ni-bearing ultramafic body and associated dolerite dykes in Longshoushan region, the southern Alashan block, were also demonstrated as products of this potential mantle superplume activity (e.g., Li et al., 2005, Fig. 1a). These Neoproterozoic intrusions suggested that the Alashan block is unlikely to be the west part of the North China Craton, but sensu lato a fragment of Rodinia with affinities to the Qilian block in the south (Dan et al., 2012; Song et al., 2012).

Two apparently distinct, sub-parallel, paleo-subduction zones have been recognized along the northern margin of the Tibetan Plateau: the North Qilian Suture Zone (oceanic-type) with ophiolitic mélanges and high-pressure eclogites and blueschists in the north (e.g., Wu et al., 1993; Song et al., 2007, 2009; C.L. Zhang et al., 2007; J.X. Zhang et al., 2007), and the North Qaidam ultrahigh-pressure metamorphic (UHPM) belt (continental-type) in the south, comprising granitic and pelitic gneisses, eclogites and garnet peridotites.

The Qilian-Qaidam mountain-basin system is truncated to the west by the Altyn Tagh fault, one of the largest strike-slip fault systems in the world (Fig. 1a). By comparing the lithologies and litho-stratigraphic associations on both sides of the Altyn Tagh fault (e.g., the lithologic units, both oceanic- and continental-type HP and UHP belts, ages of HP–UHP metamorphism), it has been suggested that ~400 km of left-lateral displacement occurred along this fault zone (e.g., Zhang et al., 2001b). Consequently, the Qaidam-Qilian-Alashan blocks are the east extension of the Tarim block.

The North Qaidam *continental-type* UHPM belt occurs as three major terranes and extends discontinuously for ~400 km between the Qaidam block in the south and the Qilian block in the north (Fig. 1b). It comprises four major rock types: (1) granitic gneiss, (2) pelitic gneiss, (3) eclogite blocks and (4) peridotite blocks. Felsic (including granitic and pelitic) gneisses are major components and occupy >90% of the UHPM belt. It was believed to be a subducted continental crust to depths of 100–200 km and exhumation in the period of ~460–400 Ma (Song et al., 2003, 2005, 2006, 2011; Mattinson et al., 2006, 2009; J.X. Zhang et al., 2006, 2008, 2010; G.B. Zhang et al., 2008; D.L. Chen et al., 2009).

3. Sample petrography

3.1. Granitic gneiss

In the North Qaidam UHP belt, granitic gneisses are the major component that occupies >80% of the whole UHPM belt. They host relatively minor eclogite, peridotite and meta-pelite blocks. The gneisses are light colored with a mineral assemblage of plagioclase, K-feldspar, quartz, and muscovite plus garnet and tourmaline present in some samples. All these granitic gneisses are deformed or mylonized with penetrated foliation and isoclinal folds (Fig. 2a,b). Most granitic gneisses preserve no high-pressure mineral assemblages perhaps due to recrystallization. Rare relic high-pressure inclusions and predicted conditions of garnet growth suggest that the orthogneiss followed a metamorphic P–T path comparable to that of the hosted eclogite with peak pressure at ~2.6 GPa close to the quartz–coesite phase boundary (Menold et al., 2009).

3.2. Pelitic gneiss

Paragneisses include garnet- (kyanite-) bearing muscovite-biotite quartz schist, garnet-free muscovite-biotite quartz schist and minor muscovite-bearing quartzite. Large eclogite blocks are always intercalated with meta-pelitic rocks. Samples (Q7-24, 25) from the Xitieshan terrane are pelitic gneisses and contain garnet (10–20%), biotite (5–10%), muscovite (10–20%), kyanite (5–10%) and accessory minerals (e.g., zircon, monazite and allanite) in addition to quartz and sodic plagioclase (Fig. 2c,e). Garnet occurs as porphyroblasts and is Alm-rich (up to 80 mol%). Sample (2C123) from Yuka terrane is a psammitic gneiss or metasandstone and consists predominantly of quartz (~80–85%) with less garnet (~5–8%) and phengitic muscovite (~10%) (Fig. 2d,f). Most pelitic gneisses in this belt have undergone HP/UHP metamorphism at ~460–420 Ma as shown by zircon geochronology (e.g., Yang et al., 2002; Song et al., 2003, 2006; Mattinson et al., 2006, 2009; J.X. Zhang et al., 2006, 2008; G.B. Zhang et al., 2008; D.L. Chen et al., 2009).

4. Zircon dating results

Measurements of U, Th and Pb for zircons from meta-pelite were conducted using the Cameca IMS-1280 secondary ion mass spectrometer (SIMS) at the Institute of Geology and Geophysics, Chinese Academy of Sciences in Beijing, and for zircons from granitic gneisses using a Quadruppole LA-ICPMS at China University of Geoscience in Beijing. Operation conditions and data reduction procedures for Cameca IMS-1280 analyses are similar to those described by Li et al. (2009b). U–Th–Pb ratios and absolute abundances were determined relative to the zircon standard 91500 (Wiedenbeck et al., 1995), which was analyzed interspersedly with unknowns. A long-term uncertainty of 1.5% (1 RSD) for $^{206}Pb/^{238}U$ measurements of the standard zircons was propagated to the unknowns (Li et al., 2010), despite that the measured $^{206}Pb/^{238}U$ error in a specific session is generally around 1% (1 RSD) or less. Measured compositions were corrected for common Pb using non-radiogenic ^{204}Pb. Corrections are sufficiently small and are insensitive to the choice of common Pb composition. An average of present-day crustal composition (Stacey and Kramers, 1975) is used for the common Pb assuming that the common Pb is largely from surface contamination introduced during sample preparation. Analytical procedures of LA-ICPMS have been described in Song et al. (2010a,b). The data are given in Tables 1 and 2. Uncertainties on individual analyses are reported using 1σ errors, and weighted mean ages for pooled $^{206}Pb/^{238}U$ results are quoted at a 95% confidence level.

4.1. Magmatic ages of the granitic gneiss

Six granitic gneiss samples from the three major blocks of the North Qaidam UHP metamorphic belt were selected for zircon geochronologic study (see Fig. 1b for sample localities). All zircons recovered from these samples are colorless, euhedral crystals with long axes varying from 100 μm to 250 μm and length/width ratios from 1.5 to 4. Cathodoluminescent (CL) images show these zircons have relatively homogeneous inner structure with clear magmatic oscillatory bands with very narrow metamorphic rims (Fig. 3).

U–Pb analyses for zircons from the granitic gneiss sample (DL31) in the Dulan terrane, the east end of the North Qaidam

Table 1
U–Th–Pb LA-ICPMS zircon data of the granitic gneiss samples.

Analysis	^{232}Th	^{238}U	Th/U	Pb	^{207}Pb/^{206}Pb	1σ	^{207}Pb/^{235}U	1σ	^{206}Pb/^{238}U	1σ	^{207}Pb/^{206}Pb Age (Ma)	1σ	^{207}Pb/^{235}U Age (Ma)	1σ	^{206}Pb/^{238}U Age (Ma)	1σ
Q7-26-01	5.15	15.09	0.34	6.88	0.07207	0.00242	1.42043	0.04599	0.1429	0.00197	988	43	898	19	861	11
Q7-26-02	5.47	14.47	0.28	7.20	0.07001	0.00232	1.48616	0.0474	0.15391	0.0021	929	43	925	19	923	12
Q7-26-03	4.88	19.12	0.12	9.10	0.07264	0.00236	1.52199	0.04771	0.15193	0.00206	1004	42	939	19	912	12
Q7-26-04	3.22	31.77	0.18	13.44	0.07163	0.00234	1.39335	0.04375	0.14104	0.00191	975	42	886	19	851	11
Q7-26-05	6.09	22.52	0.08	9.93	0.07147	0.00235	1.3806	0.04374	0.14007	0.00191	971	42	881	19	845	11
Q7-26-06	5.24	15.49	0.43	7.28	0.07146	0.00239	1.44241	0.04639	0.14636	0.00201	971	43	907	19	881	11
Q7-26-07	3.8	16.91	0.43	6.64	0.06905	0.00243	1.20285	0.04076	0.12633	0.00177	900	47	802	19	767	10
Q7-26-08	2.37	7.42	0.31	2.99	0.06561	0.00303	1.1221	0.04928	0.12405	0.00176	794	99	764	24	754	10
Q7-26-09	3.87	15.36	0.45	6.34	0.06798	0.00242	1.23017	0.04213	0.13123	0.00184	868	48	814	19	795	10
Q7-26-10	2.8	7.99	0.14	3.97	0.07027	0.00246	1.48884	0.0501	0.15365	0.00214	936	46	926	20	921	12
Q7-26-11	2.92	13.4	0.21	5.84	0.07092	0.00251	1.37817	0.0467	0.14093	0.00197	955	46	880	20	850	11
Q7-26-12	4.47	11.05	0.09	4.98	0.07035	0.00249	1.33968	0.04537	0.1381	0.00193	939	46	863	20	834	11
Q7-26-13	3.94	10.81	0.46	4.87	0.07393	0.00263	1.41851	0.04835	0.13915	0.00195	1040	46	897	20	840	11
Q7-26-14	4.87	12.66	0.10	6.24	0.07106	0.00251	1.50276	0.05083	0.15338	0.00214	959	46	932	21	920	12
Q7-26-15	2.71	7.87	0.21	3.54	0.07063	0.00259	1.35997	0.04776	0.13964	0.00198	947	49	872	21	843	11
Q7-26-16	4.16	11.37	0.08	5.72	0.07001	0.00253	1.49948	0.05172	0.15534	0.00219	929	48	930	21	931	12
Q7-26-17	2.55	8.93	0.58	4.64	0.07374	0.00269	1.67477	0.0584	0.16472	0.00233	1034	48	999	22	983	13
Q7-26-18	2.99	12.91	0.48	5.64	0.06876	0.00289	1.31918	0.05228	0.13914	0.00196	892	89	854	23	840	11
Q7-26-19	4.49	11.82	0.19	5.82	0.07038	0.00258	1.46833	0.05146	0.15131	0.00214	939	49	917	21	908	12
Q7-26-20	5.93	15.34	0.59	7.68	0.07176	0.00261	1.52074	0.0527	0.15372	0.00217	979	48	939	21	922	12
Q7-26-21	3.04	9.42	0.15	4.10	0.06747	0.00339	1.23272	0.05932	0.13251	0.00195	852	107	816	27	802	11
Q7-26-22	3.03	18.45	0.22	8.71	0.07264	0.00269	1.53963	0.05425	0.15374	0.00218	1004	48	946	22	922	12
Q7-26-23	3.3	9.71	0.10	4.90	0.07119	0.0027	1.54907	0.05589	0.15784	0.00226	963	50	950	22	945	13
Q7-26-24	2.99	18.35	0.06	8.40	0.07107	0.00292	1.44671	0.05576	0.14764	0.00208	959	86	909	23	888	12
Q7-26-25	3.06	12.05	0.14	5.72	0.07183	0.00273	1.48515	0.05366	0.14999	0.00215	981	50	924	22	901	12
Q7-31-01	25.51	2265.63	0.14	322.94	0.06843	0.00214	1.21117	0.03512	0.12837	0.00149	882	66	806	16	779	9
Q7-31-02	58.63	6540.65	0.18	657.98	0.06965	0.00196	0.89657	0.02296	0.09337	0.00108	918	59	650	12	575	6
Q7-31-03	253.23	19847.99	0.34	1334.44	0.06383	0.00163	0.57201	0.01305	0.065	0.00074	736	55	459	8	406	4
Q7-31-04	271.41	511.84	0.28	91.79	0.07055	0.00176	1.52666	0.0371	0.15691	0.00189	944	30	941	15	940	11
Q7-31-05	41.48	3816.42	0.12	494.58	0.06946	0.00179	1.1924	0.02751	0.12451	0.00142	912	54	797	13	756	8
Q7-31-06	17.93	3050.94	0.18	432.36	0.06978	0.00169	1.34894	0.02875	0.14021	0.0016	922	51	867	12	846	9
Q7-31-07	21.4	2167.64	0.08	227.15	0.0634	0.00211	0.83081	0.02585	0.09504	0.00111	722	72	614	14	585	7
Q7-31-08	91.69	4150.51	0.43	536.36	0.07075	0.00201	1.17564	0.03045	0.12052	0.0014	950	59	789	14	734	8
Q7-31-09	110.98	3717.89	0.43	511.14	0.07075	0.00184	1.2902	0.03016	0.13226	0.00152	950	55	841	13	801	9
Q7-31-10	27.41	2880.12	0.31	366.93	0.06848	0.00198	1.12536	0.02985	0.11919	0.00139	883	61	766	14	726	8
Q7-31-11	106.74	352.99	0.45	46.23	0.06665	0.00194	1.09525	0.03095	0.11914	0.00151	827	38	751	15	726	9
Q7-31-12	26.51	2787.59	0.14	416.44	0.06893	0.0019	1.35248	0.0339	0.14231	0.00165	897	58	869	15	858	9
Q7-31-13	144.69	912.66	0.21	112.94	0.0709	0.00175	1.129	0.0271	0.11545	0.00138	955	30	767	13	704	8
Q7-31-14	74.69	4875.78	0.09	555.52	0.0688	0.00176	1.05923	0.02421	0.11166	0.00128	893	54	733	12	682	7
Q7-31-15	20.38	4417.94	0.46	603.62	0.07178	0.00179	1.3369	0.02958	0.13508	0.00155	980	52	862	13	817	9
Q7-31-16	166.82	417.01	0.10	71.82	0.07021	0.00184	1.50122	0.03815	0.15503	0.00189	935	32	931	15	929	11
Q7-31-17	44.99	3824.02	0.21	522.11	0.07152	0.00191	1.30906	0.03148	0.13276	0.00154	972	56	850	14	804	9
Q7-31-18	78.63	343.63	0.08	94.48	0.08132	0.00402	2.38003	0.11331	0.21227	0.00281	1229	99	1237	34	1241	15
Q7-31-19	120.87	474.77	0.58	84.66	0.07168	0.00184	1.65089	0.04094	0.16699	0.00202	977	31	990	16	996	11
Q7-31-20	85.05	5534.48	0.48	539.12	0.06589	0.0022	0.80916	0.02529	0.08906	0.00106	803	72	602	14	550	6
Q7-31-21	328.06	1262.21	0.19	150.18	0.05968	0.00274	0.81887	0.03624	0.09951	0.00124	592	102	607	20	612	7
Q7-31-22	61.71	4605.86	0.59	507.51	0.06965	0.00199	1.01666	0.02646	0.10587	0.00125	918	60	712	13	649	7
Q7-31-23	31.58	3592.84	0.15	451.69	0.06809	0.0025	1.05527	0.0366	0.11241	0.00136	871	78	731	18	687	8
Q7-31-24	17.4	1086.71	0.22	195.74	0.07142	0.00213	1.735	0.05013	0.17612	0.00226	969	38	1022	19	1046	12
Q7-31-25	264.71	936.27	0.10	134.46	0.07792	0.00215	1.37447	0.03669	0.12789	0.00159	1145	33	878	16	776	9
DL31-01	509.36	417.44	0.06	30.18	0.06901	0.00214	1.39451	0.04231	0.14653	0.00195	899	41	887	18	881	11
DL31-02	119.04	882.54	0.14	26.25	0.07017	0.00211	1.42668	0.04205	0.14744	0.00194	933	39	900	18	887	11
DL31-03	60.52	558.84	0.24	16.34	0.06847	0.00211	1.43045	0.04305	0.15148	0.00201	883	40	902	18	909	11
DL31-04	59.87	740.83	0.21	20.05	0.06878	0.00211	1.38087	0.04136	0.14558	0.00193	892	40	881	18	876	11

Table 1 (*Continued*)

Analysis	^{232}Th	^{238}U	Th/U	Pb	^{207}Pb/^{206}Pb	1σ	^{207}Pb/^{235}U	1σ	^{206}Pb/^{238}U	1σ	^{207}Pb/^{206}Pb Age (Ma)	1σ	^{207}Pb/^{235}U Age (Ma)	1σ	^{206}Pb/^{238}U Age (Ma)	1σ
DL31-05	29.92	442.28	0.78	12.26	0.06898	0.00217	1.43003	0.04391	0.15034	0.00201	898	41	902	18	903	11
DL31-06	139.47	768.46	0.18	31.31	0.07444	0.00266	1.81255	0.06006	0.1766	0.00233	1053	74	1050	22	1048	13
DL31-07	403.43	739.79	0.10	35.30	0.06907	0.00216	1.44098	0.04401	0.15129	0.00202	901	41	906	18	908	11
DL31-08	50.67	584.48	0.06	16.61	0.06904	0.00219	1.43659	0.04454	0.15089	0.00203	900	42	904	19	906	11
DL31-09	47.7	719.19	0.09	19.78	0.06971	0.0022	1.44504	0.04452	0.15031	0.00202	920	41	908	18	903	11
DL31-10	218.22	490.54	0.50	21.77	0.06956	0.00227	1.42994	0.0455	0.14906	0.00203	915	43	902	19	896	11
DL31-11	82.79	488.43	0.05	15.64	0.06995	0.00229	1.45562	0.04654	0.15089	0.00206	927	43	912	19	906	12
DL31-12	223.74	852.87	0.22	27.11	0.07177	0.00233	1.45851	0.0463	0.14736	0.00201	979	42	913	19	886	11
DL31-13	40.89	989	0.16	16.63	0.06171	0.00215	0.81889	0.02636	0.09624	0.00128	664	76	607	15	592	8
DL31-14	30.13	608.82	0.23	12.41	0.06538	0.00221	1.03368	0.03419	0.11464	0.00159	787	46	721	17	700	9
DL31-15	47.14	845.2	0.14	22.94	0.06922	0.00229	1.44025	0.04646	0.15088	0.00207	905	44	906	19	906	12
DL31-16	59.5	685.35	0.13	19.50	0.06923	0.00233	1.4387	0.04732	0.1507	0.00209	906	45	905	20	905	12
DL31-17	145.98	862.01	0.20	26.98	0.0693	0.00233	1.42072	0.0467	0.14865	0.00206	908	45	898	20	893	12
DL31-18	53.63	530.72	0.12	15.67	0.06782	0.00232	1.44104	0.04815	0.15408	0.00215	863	46	906	20	924	12
DL31-19	109.1	761.49	0.32	23.45	0.06972	0.00238	1.45358	0.04844	0.15118	0.00211	920	46	911	20	908	12
DL31-20	77.96	901.61	0.70	24.39	0.06847	0.00236	1.38253	0.04649	0.14642	0.00205	883	46	882	20	881	12
DL31-21	63.04	1019.98	0.28	27.36	0.07063	0.00246	1.41858	0.04828	0.14565	0.00205	947	47	897	20	877	12
DL31-22	56.78	1291.84	0.29	34.24	0.06905	0.00241	1.42036	0.04843	0.14917	0.00211	900	47	898	20	896	12
DL31-23	44.48	886.43	0.36	22.46	0.06762	0.0025	1.33422	0.04807	0.14307	0.00207	857	51	861	21	862	12
DL31-24	287.33	907.57	0.28	32.37	0.06896	0.00246	1.39718	0.04869	0.14693	0.0021	898	48	888	21	884	12
DL31-25	629.3	735.45	0.77	25.83	0.06868	0.00251	1.39847	0.04983	0.14765	0.00213	889	50	888	21	888	12
09Q13-01	100.17	860.09	0.56	138.96	0.07121	0.0021	1.52516	0.04619	0.15537	0.0021	963	40	941	19	931	12
09Q13-02	138.28	1126.02	0.22	183.80	0.0701	0.00207	1.51681	0.04597	0.15699	0.00212	931	40	937	19	940	12
09Q13-03	75.74	606.82	0.14	96.59	0.06979	0.00209	1.47294	0.04526	0.1531	0.00207	922	41	919	19	918	12
09Q13-04	102.08	517.13	0.18	139.88	0.10493	0.0036	3.55377	0.1122	0.24562	0.0033	1713	65	1539	25	1416	17
09Q13-05	2291.59	537.56	0.34	112.96	0.0699	0.00212	1.22511	0.03817	0.12716	0.00173	925	42	812	17	772	10
09Q13-06	169.12	750.07	0.28	117.97	0.07208	0.00218	1.48669	0.0461	0.14962	0.00202	988	41	925	19	899	11
09Q13-07	83.98	370.62	0.12	58.05	0.07035	0.00218	1.43223	0.04555	0.14769	0.00201	939	43	902	19	888	11
09Q13-08	83.64	251.27	0.18	43.47	0.07054	0.00225	1.54597	0.05045	0.15898	0.00219	944	44	949	20	951	12
09Q13-09	95.8	352.69	0.08	60.46	0.07056	0.00221	1.55258	0.04972	0.15962	0.00218	945	43	952	20	955	12
09Q13-10	54.7	272.34	0.43	45.78	0.07046	0.00224	1.54142	0.05013	0.15871	0.00218	942	44	947	20	950	12
09Q13-11	109.59	1436.54	0.43	222.28	0.07003	0.00241	1.44426	0.04579	0.14957	0.00198	929	72	907	19	899	11
09Q13-12	97.16	276.77	0.31	48.11	0.06943	0.00223	1.51772	0.04978	0.15858	0.00218	912	45	938	20	949	12
09Q13-13	161.21	559.36	0.45	85.26	0.07068	0.00222	1.4099	0.04541	0.1447	0.00197	948	44	893	19	871	11
09Q13-14	67.84	347.74	0.14	55.68	0.06861	0.00222	1.43411	0.04738	0.15163	0.00208	887	46	903	20	910	12
09Q13-15	50.24	248.98	0.21	42.29	0.06974	0.0023	1.54499	0.05206	0.16072	0.00222	921	46	948	21	961	12
09Q13-16	53.99	520.78	0.09	77.32	0.07134	0.0023	1.41769	0.04666	0.14416	0.00197	967	45	896	20	868	11
09Q13-17	93.49	945.2	0.46	144.07	0.06971	0.00222	1.42362	0.04633	0.14814	0.00201	920	45	899	19	891	11
09Q13-18	239.84	1700.94	0.10	275.51	0.06924	0.00219	1.48712	0.04821	0.15581	0.00211	906	44	925	20	933	12
09Q13-19	156.23	1301.36	0.21	206.81	0.07097	0.00226	1.50381	0.04904	0.1537	0.00209	957	44	932	20	922	12
09Q13-20	676.61	686.7	0.08	88.34	0.06757	0.00222	0.82716	0.02779	0.0888	0.00122	855	47	612	15	548	7
09Q13-21	112.61	1101.63	0.58	157.46	0.06969	0.00226	1.33234	0.04419	0.13868	0.00189	919	46	860	19	837	11
09Q13-22	142.02	582.38	0.48	94.48	0.0709	0.00233	1.52089	0.05109	0.1556	0.00213	955	46	939	21	932	12
09Q13-23	166.11	1534.97	0.19	249.08	0.06968	0.00227	1.51455	0.05044	0.15766	0.00215	919	46	936	20	944	12
09Q13-24	61.94	255.64	0.59	43.79	0.06984	0.0024	1.54825	0.05415	0.1608	0.00223	924	49	950	22	961	12
09Q13-25	115.21	983.8	0.15	140.38	0.069	0.00269	1.28573	0.04699	0.13515	0.00182	899	82	839	21	817	10
09Q13-26	168.16	245.98	0.22	43.25	0.07306	0.00466	1.37171	0.08499	0.13617	0.00206	1016	133	877	36	823	12
09Q13-27	144.33	1608.93	0.10	230.84	0.0692	0.00281	1.28458	0.04916	0.13463	0.00182	905	86	839	22	814	10
09Q13-28	98.16	449.65	0.06	57.07	0.06771	0.00292	1.09202	0.04465	0.11697	0.00162	860	92	749	22	713	9
09Q13-29	304.54	431.35	0.14	172.42	0.11532	0.00389	5.21546	0.17948	0.32806	0.0045	1885	42	1855	29	1829	22
09Q13-30	90.7	927.86	0.24	146.01	0.07013	0.00238	1.48419	0.05148	0.1535	0.0021	932	49	924	21	921	12
09Q25-01	72.56	394.81	0.21	63.71	0.07001	0.00245	1.48106	0.05272	0.15344	0.00212	929	50	923	22	920	12
09Q25-02	47.84	469.22	0.78	101.82	0.08756	0.00325	2.50782	0.08676	0.20772	0.0028	1373	73	1274	25	1217	15
09Q25-03	224.08	553.57	0.18	81.70	0.06874	0.00241	1.25133	0.04466	0.13203	0.00182	891	51	824	20	799	10
09Q25-04	546.97	466.53	0.10	121.06	0.08229	0.00287	2.18841	0.07788	0.19288	0.00266	1252	48	1177	25	1137	14

Table 1 (*Continued*)

Analysis	^{232}Th	^{238}U	Th/U	Pb	^{207}Pb/^{206}Pb	1σ	^{207}Pb/^{235}U	1σ	^{206}Pb/^{238}U	1σ	^{207}Pb/^{206}Pb Age (Ma)	1σ	^{207}Pb/^{235}U Age (Ma)	1σ	^{206}Pb/^{238}U Age (Ma)	1σ
09Q25-05	31.95	324.04	0.06	54.35	0.07084	0.00254	1.59897	0.05821	0.16371	0.00227	953	52	970	23	977	13
09Q25-06	68.39	311.41	0.09	49.31	0.07206	0.00264	1.48491	0.05528	0.14947	0.00208	988	53	924	23	898	12
09Q25-07	82.05	1244.87	0.50	201.74	0.06949	0.00285	1.48307	0.05744	0.15479	0.0021	913	87	923	23	928	12
09Q25-08	114.22	307.48	0.05	59.26	0.07559	0.00275	1.80158	0.06666	0.17287	0.00241	1084	52	1046	24	1028	13
09Q25-09	115.72	339.42	0.22	86.07	0.11056	0.00464	3.39143	0.13413	0.22248	0.00312	1809	78	1502	31	1295	16
09Q25-10	87.67	316.29	0.16	53.34	0.07089	0.00262	1.53279	0.05754	0.15683	0.00219	954	54	944	23	939	12
09Q25-11	63.04	517.94	0.23	81.98	0.07063	0.0026	1.49427	0.05587	0.15345	0.00213	947	54	928	23	920	12
09Q25-12	51.25	284.26	0.14	47.95	0.06996	0.00263	1.56017	0.05955	0.16175	0.00227	927	55	955	24	966	13
09Q25-13	74.87	942.22	0.13	125.34	0.06518	0.00394	1.02109	0.06002	0.11362	0.00161	780	131	714	30	694	9
09Q25-14	69.56	163.24	0.20	29.30	0.07253	0.00283	1.61662	0.06379	0.16165	0.00229	1001	57	977	25	966	13
09Q25-15	131.06	305.86	0.12	54.22	0.07047	0.00267	1.54401	0.05944	0.15891	0.00223	942	56	948	24	951	12
09Q25-16	116.57	371.41	0.32	63.72	0.0717	0.00273	1.56657	0.06062	0.15846	0.00222	977	56	957	24	948	12
09Q25-17	106.82	235.96	0.70	42.04	0.07076	0.00275	1.55924	0.06146	0.15982	0.00225	950	57	954	24	956	13
09Q25-18	44.13	311.49	0.28	51.94	0.06959	0.0027	1.54984	0.06093	0.16151	0.00227	916	58	950	24	965	13
09Q25-19	78.7	373.26	0.29	60.73	0.07033	0.00272	1.49839	0.05873	0.15451	0.00216	938	57	930	24	926	12
09Q25-20	58	642.19	0.36	100.22	0.06932	0.00267	1.46345	0.05718	0.15312	0.00214	908	57	915	24	918	12
09Q25-21	109.67	239.36	0.28	38.74	0.07434	0.00298	1.50725	0.06113	0.14704	0.00209	1051	59	933	25	884	12
09Q25-22	128.68	1264.96	0.77	196.30	0.06996	0.00319	1.41213	0.06135	0.14639	0.00201	927	96	894	26	881	11
09Q25-23	96.98	468.3	0.56	75.33	0.07157	0.00281	1.50341	0.05996	0.15235	0.00214	974	58	932	24	914	12
09Q25-24	84.59	1036.67	0.22	157.14	0.07003	0.00309	1.40338	0.05883	0.14534	0.00199	929	93	890	25	875	11
09Q25-25	255.17	442.21	0.14	76.85	0.07268	0.00288	1.50351	0.06042	0.15002	0.00211	1005	59	932	25	901	12
09Q25-26	91.6	192.15	0.18	33.12	0.06946	0.00289	1.48181	0.06241	0.15471	0.00221	912	63	923	26	927	12
09Q25-27	55.33	299.04	0.34	52.63	0.10269	0.00415	2.15125	0.08809	0.15193	0.00215	1673	55	1165	28	912	12
09Q25-28	128.39	218.16	0.28	43.62	0.07781	0.00319	1.86066	0.07725	0.17341	0.00246	1142	60	1067	27	1031	14
09Q25-29	48.48	315.03	0.12	51.00	0.0715	0.00293	1.54065	0.06394	0.15625	0.00221	972	61	947	26	936	12
09Q25-30	124.88	572.11	0.18	95.03	0.07061	0.00287	1.53553	0.06335	0.15772	0.00222	946	61	945	25	944	12
09Q30-01	85.81	877.76	0.08	139.54	0.07106	0.00193	1.48994	0.04183	0.15215	0.00203	959	36	926	17	913	11
09Q30-02	74.21	1168.13	0.43	178.98	0.07101	0.00229	1.42542	0.04209	0.1456	0.00191	958	68	900	18	876	11
09Q30-03	286.51	2031	0.43	298.90	0.07165	0.00193	1.39152	0.03879	0.14092	0.00188	976	35	885	16	850	11
09Q30-04	179.92	745	0.31	126.62	0.07045	0.00192	1.52131	0.04288	0.15669	0.0021	941	36	939	17	938	12
09Q30-05	159.68	758.73	0.45	118.73	0.07401	0.00203	1.50535	0.0427	0.14759	0.00198	1042	36	933	17	887	11
09Q30-06	743.61	951.83	0.14	140.89	0.07142	0.00196	1.32009	0.03747	0.13411	0.0018	969	36	855	16	811	10
09Q30-07	162.25	911.91	0.21	139.33	0.07137	0.00195	1.42173	0.04016	0.14455	0.00193	968	36	898	17	870	11
09Q30-08	144.62	1471.32	0.09	205.55	0.07025	0.00227	1.28593	0.03797	0.13277	0.00175	936	68	839	17	804	10
09Q30-09	34.32	609.38	0.46	100.61	0.07005	0.00193	1.55134	0.0442	0.16068	0.00216	930	37	951	18	961	12
09Q30-10	58.56	647.9	0.10	102.99	0.06986	0.00193	1.47597	0.04201	0.15331	0.00206	924	37	921	17	919	12
09Q30-11	262.59	526.68	0.21	91.98	0.06911	0.00193	1.45192	0.0418	0.15242	0.00205	902	37	911	17	915	11
09Q30-12	44.16	808.33	0.08	127.97	0.06918	0.00191	1.47241	0.04192	0.15443	0.00207	904	37	919	17	926	12
09Q30-13	231.81	1043.42	0.58	163.31	0.07129	0.00197	1.44494	0.0413	0.14706	0.00197	966	37	908	17	884	11
09Q30-14	160.53	999.18	0.48	150.29	0.07068	0.00195	1.3973	0.0399	0.14344	0.00192	948	37	888	17	864	11
09Q30-15	176.99	770.74	0.19	109.75	0.06593	0.00243	1.18697	0.04064	0.13058	0.00176	804	79	795	19	791	10
09Q30-16	80.8	584.8	0.59	94.28	0.06983	0.00197	1.48107	0.04303	0.15388	0.00207	923	38	923	18	923	12
09Q30-17	256.52	1958.47	0.15	282.82	0.06945	0.00235	1.29949	0.04048	0.1357	0.0018	912	71	845	18	820	10
09Q30-18	173.67	881.84	0.22	136.53	0.07161	0.00201	1.45152	0.04201	0.14706	0.00197	975	37	911	17	884	11
09Q30-19	87.54	757.57	0.10	120.14	0.07188	0.00245	1.49405	0.04693	0.15075	0.00202	983	71	928	19	905	11
09Q30-20	181.05	558.25	0.06	83.60	0.07684	0.00222	1.39921	0.04164	0.13211	0.00179	1117	38	889	18	800	10
09Q30-21	247.8	354.46	0.14	65.71	0.06852	0.002	1.47448	0.04433	0.15612	0.00211	884	40	920	18	935	12
09Q30-22	460.67	1618.42	0.24	228.73	0.06785	0.00191	1.23159	0.03584	0.1317	0.00177	864	38	815	16	798	10
09Q30-23	385.16	1345.47	0.21	180.07	0.07677	0.00218	1.32321	0.03869	0.12504	0.00168	1115	37	856	17	760	10
09Q30-24	118.97	331.76	0.78	56.10	0.06757	0.002	1.43346	0.04358	0.15391	0.00209	855	41	903	18	923	12
09Q30-25	167.42	598.52	0.18	101.62	0.07043	0.00203	1.52164	0.04522	0.15674	0.00211	941	39	939	18	939	12
09Q30-26	664.76	866.15	0.10	112.62	0.0743	0.00371	1.07216	0.05119	0.10466	0.00152	1050	103	740	25	642	9
09Q30-27	128.07	228.02	0.06	38.90	0.07048	0.00218	1.43061	0.04529	0.14726	0.00202	942	42	902	19	886	11
09Q30-28	140.05	626.04	0.09	97.42	0.0712	0.00256	1.41588	0.04719	0.14422	0.00194	963	75	896	20	868	11
09Q30-29	94.8	694.3	0.50	107.72	0.07065	0.00207	1.44723	0.04355	0.14861	0.002	947	40	909	18	893	11
09Q30-30	144.08	819.01	0.05	128.30	0.07115	0.00207	1.45323	0.0436	0.14819	0.002	962	39	911	18	891	11

Table 2
U–Th–Pb analytical data and derived ages measured by secondary ion mass spectrometry (SIMS).

Sample/spot #	[U] (ppm)	[Th] (ppm)	[Pb] (ppm)	Th/U (meas)	$^{207}Pb/^{235}U$	$\pm\sigma$ (%)	$^{206}Pb/^{238}U$	$\pm\sigma$ (%)	$^{207}Pb/^{206}Pb$	$\pm\sigma$ (%)	$^{207}Pb/^{206}Pb$	$\pm\sigma$	$^{207}Pb/^{235}U$	$\pm\sigma$	$^{206}Pb/^{238}U$	$\pm\sigma$
2C123@1	945	40	158	0.043	1.47206	1.57	0.1544	1.50	0.06914	0.44	903.0	9.1	919.0	9.5	925.7	13.0
2C123@2	826	25	135	0.030	1.46052	1.57	0.1512	1.50	0.07004	0.44	929.5	9.0	914.2	9.5	907.9	12.7
2C123@3	604	207	202	0.342	3.89655	1.56	0.2773	1.51	0.10191	0.41	1659.3	7.6	1613.0	12.7	1577.7	21.1
2C123@4	852	29	139	0.034	1.44587	1.57	0.1511	1.50	0.06940	0.44	910.7	9.1	908.2	9.5	907.1	12.7
2C123@5	903	29	148	0.032	1.44909	1.56	0.1514	1.51	0.06940	0.42	910.8	8.7	909.5	9.4	909.0	12.8
2C123@6	1649	108	272	0.066	1.45524	1.58	0.1521	1.51	0.06941	0.46	911.0	9.5	912.0	9.6	912.5	12.9
2C123@7	699	118	119	0.168	1.44490	1.58	0.1519	1.50	0.06899	0.49	898.3	10.1	907.8	9.5	911.6	12.8
2C123@8	815	86	128	0.105	1.37637	1.59	0.1433	1.50	0.06964	0.53	917.7	11.0	878.9	9.4	863.6	12.1
2C123@9	930	28	170	0.030	1.62637	1.61	0.1696	1.52	0.06957	0.53	915.6	10.8	980.5	10.2	1009.7	14.2
2C123@10	616	44	101	0.072	1.43232	1.62	0.1510	1.51	0.06878	0.60	892.1	12.3	902.5	9.7	906.8	12.8
2C123@11	175	100	66	0.571	4.61660	1.65	0.2957	1.51	0.11322	0.65	1851.7	11.8	1752.3	13.8	1670.2	22.3
2C123@12	440	194	68	0.442	1.37340	1.93	0.1434	1.52	0.06947	1.18	912.6	24.1	877.6	11.4	863.8	12.3
2C123@13	489	100	138	0.205	3.12373	1.65	0.2473	1.50	0.09162	0.70	1459.6	13.2	1438.6	12.8	1424.4	19.2
2C123@15	825	23	144	0.028	1.56033	1.71	0.1619	1.58	0.06989	0.66	925.2	13.6	954.6	10.6	967.4	14.2
2C123@17	354	36	59	0.102	1.43390	1.84	0.1504	1.52	0.06915	1.05	903.3	21.5	903.2	11.1	903.1	12.8
2C123@18	1048	39	168	0.037	1.41380	1.56	0.1482	1.50	0.06919	0.41	904.4	8.4	894.8	9.3	890.8	12.5
2C123@19	1277	243	320	0.190	2.69765	1.54	0.2188	1.51	0.08941	0.30	1412.9	5.6	1327.8	11.5	1275.7	17.5
2C123@20	760	88	124	0.116	1.42844	1.66	0.1483	1.56	0.06984	0.57	923.7	11.7	900.9	10.0	891.6	13.0
2C123@21	502	86	84	0.172	1.42795	1.63	0.1489	1.50	0.06957	0.64	915.7	13.1	900.7	9.8	894.6	12.6
2C123@22	482	136	107	0.282	2.16815	1.72	0.1863	1.51	0.08442	0.83	1302.2	16.0	1170.9	12.1	1101.2	15.3
2C123@23	1274	172	281	0.135	2.23507	1.59	0.1925	1.52	0.08420	0.48	1297.1	9.3	1192.1	11.2	1135.1	15.8
2C123@24	351	196	124	0.557	4.02748	1.63	0.2789	1.56	0.10474	0.44	1709.8	8.1	1639.8	13.3	1585.7	22.0
2C123@25	816	107	194	0.131	2.68305	1.59	0.2094	1.50	0.09293	0.51	1486.4	9.7	1323.8	11.8	1225.6	16.8
2C123@26	707	34	114	0.048	1.42243	1.71	0.1489	1.51	0.06930	0.82	907.6	16.7	898.4	10.3	894.6	12.6
2C123@27	648	94	107	0.145	1.41859	1.59	0.1489	1.50	0.06910	0.54	901.8	11.0	896.8	9.5	894.7	12.5
2C123@28	540	140	92	0.259	1.42374	1.72	0.1494	1.50	0.06911	0.84	902.1	17.2	898.9	10.3	897.6	12.6
2C123@29	707	21	117	0.030	1.46814	1.60	0.1535	1.53	0.06937	0.48	909.8	9.9	917.4	9.7	920.5	13.1
Q7-24@01	424	133	75	0.313	1.46658	1.59	0.1524	1.50	0.06999	0.51	922.6	10.8	916.7	9.6	914.3	12.8
Q7-24@02	328	61	53	0.187	1.36222	1.78	0.1449	1.50	0.07326	0.70	874.6	19.8	872.8	10.5	872.1	12.3
Q7-24@03	389	67	65	0.172	1.42430	1.60	0.1491	1.51	0.06946	0.54	907.2	11.4	899.2	9.6	895.9	12.6
Q7-24@04	417	71	68	0.171	1.38574	1.60	0.1460	1.50	0.06883	0.54	893.7	11.2	882.9	9.5	878.6	12.3
Q7-24@05	400	60	63	0.150	1.34101	1.78	0.1407	1.50	0.06996	0.91	902.9	19.5	863.7	10.4	848.5	11.9
Q7-24@06	362	53	59	0.147	1.39226	1.61	0.1463	1.50	0.06916	0.58	899.5	12.1	885.7	9.6	880.1	12.4
Q7-24@07	497	62	83	0.126	1.43426	1.64	0.1504	1.50	0.06954	0.64	903.8	13.4	903.3	9.8	903.1	12.7
Q7-24@08	613	43	97	0.071	1.39258	1.57	0.1447	1.50	0.06980	0.45	922.5	9.2	885.8	9.3	871.2	12.2
Q7-24@09	559	68	88	0.122	1.35076	1.58	0.1420	1.50	0.06936	0.47	898.4	10.1	867.9	9.3	856.0	12.0
Q7-24@10	424	39	68	0.093	1.38634	1.63	0.1456	1.50	0.06904	0.64	899.9	13.2	883.1	9.7	876.5	12.3
Q7-24@11	547	69	88	0.125	1.40746	1.58	0.1459	1.51	0.07017	0.47	927.6	9.8	892.1	9.4	877.8	12.4
Q7-24@12	562	135	96	0.240	1.30101	1.58	0.1368	1.50	0.06940	0.47	897.3	10.3	846.2	9.1	826.8	11.7
Q7-24@13	424	61	67	0.143	1.35354	1.61	0.1430	1.50	0.06943	0.55	888.7	12.3	869.1	9.5	861.4	12.1
Q7-24@14	397	50	39	0.126	0.75263	1.74	0.0889	1.50	0.06198	0.84	654.1	18.9	569.8	7.6	548.8	7.9
Q7-24@15	324	48	53	0.150	1.40023	1.63	0.1460	1.50	0.06980	0.61	915.0	13.0	889.0	9.7	878.6	12.3
Q7-24@15	324	48	53	0.150	1.40023	1.63	0.1460	1.50	0.06980	0.61	915.0	13.0	889.0	9.7	878.6	12.3
Q7-24@16	313	46	53	0.146	1.44269	1.62	0.1513	1.50	0.06914	0.60	902.9	12.4	906.8	9.7	908.5	12.7
Q7-25@01	373	65	62	0.175	1.41951	1.62	0.1479	1.51	0.06961	0.57	917.0	11.7	897.2	9.7	889.1	12.6
Q7-25@02	386	54	66	0.139	1.46858	1.63	0.1527	1.50	0.06986	0.61	920.6	12.7	917.5	9.9	916.3	12.8
Q7-25@03	298	49	46	0.164	1.33041	1.67	0.1388	1.51	0.07011	0.68	914.7	14.5	859.1	9.7	837.6	11.9
Q7-25@04	444	72	71	0.162	1.37006	1.62	0.1421	1.50	0.06992	0.61	926.0	12.4	876.2	9.5	856.6	12.0
Q7-25@05	306	44	47	0.144	1.33028	1.71	0.1389	1.50	0.06986	0.80	912.8	16.9	859.0	10.0	838.3	11.8
Q7-25@06	410	45	60	0.109	1.28317	1.61	0.1328	1.50	0.07008	0.60	930.8	12.2	838.3	9.3	803.8	11.3
Q7-25@07	433	67	68	0.154	1.35124	1.61	0.1411	1.50	0.06958	0.57	912.0	11.8	868.1	9.4	851.0	12.0
Q7-25@08	668	54	106	0.081	1.38117	1.58	0.1450	1.50	0.07002	0.43	900.7	9.9	880.9	9.3	873.1	12.3
Q7-25@09	359	44	57	0.124	1.36217	1.67	0.1432	1.50	0.07022	0.65	898.9	14.8	872.8	9.8	862.6	12.1
Q7-25@10	392	46	62	0.117	1.37137	1.61	0.1437	1.50	0.06924	0.58	905.8	11.9	876.8	9.5	865.3	12.2
Q7-25@11	365	49	58	0.133	1.37886	1.84	0.1426	1.50	0.07224	0.98	932.1	21.7	880.0	10.9	859.3	12.1
Q7-25@12	460	107	80	0.233	1.47304	1.58	0.1529	1.50	0.07000	0.50	924.6	10.3	919.4	9.6	917.2	12.9
Q7-25@13	372	53	60	0.143	1.39953	1.65	0.1445	1.50	0.07210	0.57	936.0	14.1	888.7	9.8	869.9	12.2
Q7-25@14	294	50	49	0.170	1.41612	2.07	0.1478	1.51	0.06951	1.42	913.8	29.0	895.7	12.4	888.4	12.5
Q7-25@15	388	63	61	0.163	1.33590	1.70	0.1400	1.50	0.06921	0.79	905.0	16.2	861.4	9.9	844.6	11.9
Q7-25@16	310	48	49	0.155	1.36688	1.65	0.1427	1.50	0.06983	0.63	912.2	13.9	874.8	9.7	860.1	12.1

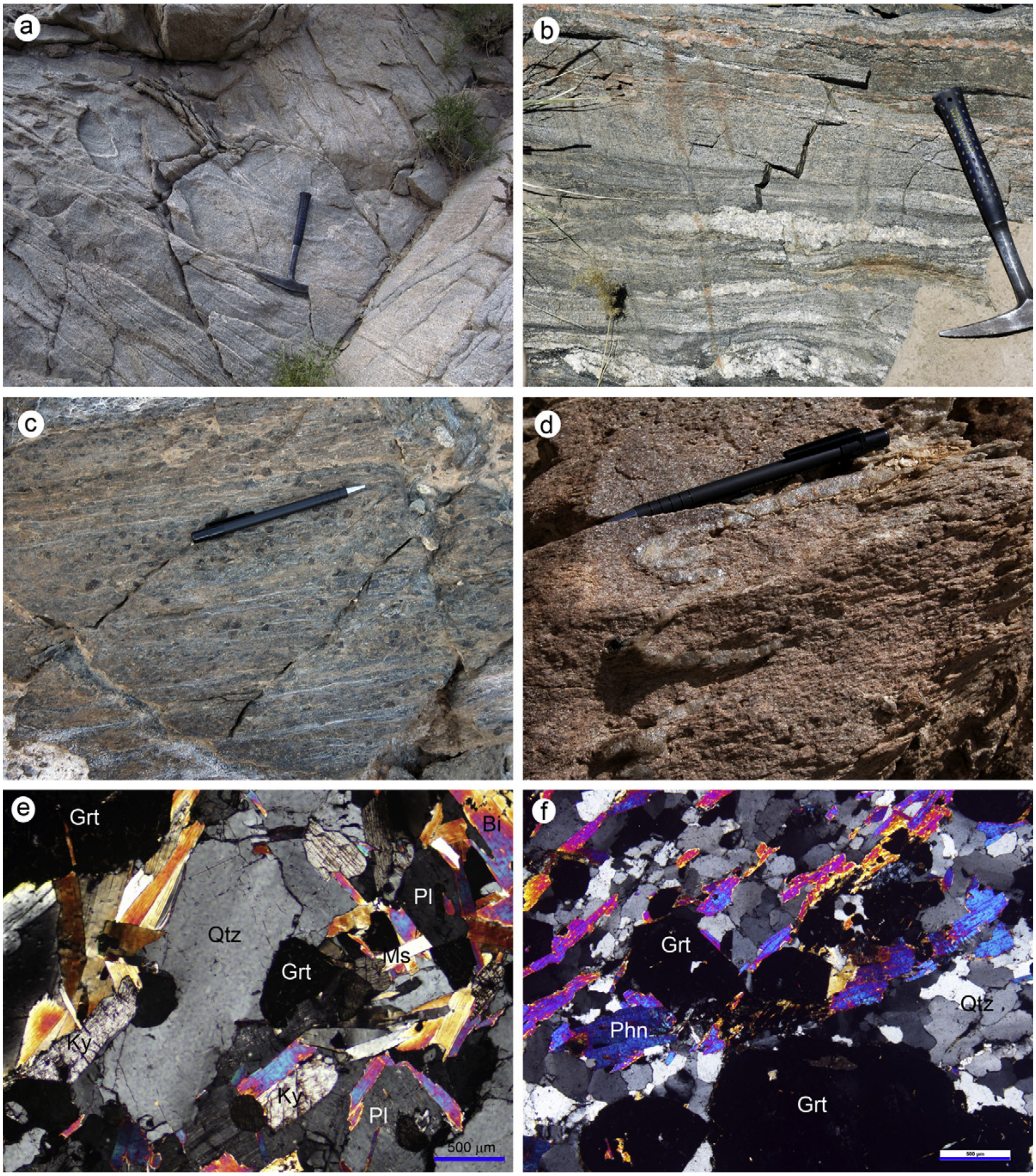

Fig. 2. Photographs showing field and micro-structure of the studied granitic and pelitic/psammitic gneisses in the North Qaidam UHPM belt. (a) Granitic gneiss with strong foliations in the Yuka terrane. (b) Granitic gneiss with felsic melts in the Xitieshan terrane. (c) Pelitic gneiss with garnet and kyanite in the Xitieshan terrane. (d) Psammitic gneiss with garnet and phengitic mica in the Yuka terrane. (e) Pelitic gneiss with mineral assemblage of garnet (Grt), kyanite (Ky), biotite (Bi), muscovite (Ms), Plagioclase (Pl) and quartz (Qtz) (Sample Q7-24). (f) Garnet, phengite (Phn) and quartz mineral assemblage of psammitic gneiss (Sample 2C123).

UHPM belt, form an approximately concordant population with a mean $^{207}Pb/^{206}Pb$ age of 907 ± 18 Ma ($n = 22$, MSWD = 0.36) (Fig. 4a). Zircon grains ($n = 28$) from the other sample (9Q13) in Dulan terrane form a discordant mixing line with upper intercepts at 936 ± 28 Ma (MSWD = 0.18) and a mean $^{207}Pb/^{206}Pb$ age of 932 ± 18 Ma (MSWD = 0.37) (Fig. 4b). One inherited core gives a concordant age of 1885 ± 42 Ma.

U–Pb analyses for zircons from two granitic gneiss samples (9Q25, 9Q30) in the Xitieshan terrane yield upper intercepts at 953 ± 40 Ma (MSWD = 0.28) and 935 ± 25 Ma (MSWD = 0.67) with mean $^{207}Pb/^{206}Pb$ ages of 951 ± 24 Ma ($n = 23$, MSWD = 0.41) and 942 ± 16 Ma ($n = 26$, MSWD = 0.42), respectively (Fig. 4c,d). Two granitic gneiss samples (Q7-26, Q7-31) from the Yuka terrane give similar ages of upper intercepts [1002 ± 80 Ma (MSWD = 0.39) and 949 ± 33 Ma (MSWD = 0.56)] and $^{207}Pb/^{206}Pb$ weighted means [976 ± 19 Ma ($n = 22$, MSWD = 0.63) and 941 ± 21 Ma ($n = 18$, MSWD = 0.45)] (Fig. 4e–g). Therefore, the protoliths of the major granitic gneiss within the North Qaidam UHPM belt must have formed in the time period of 1000–910 Ma.

4.2. Metamorphic ages of pelitic gneisses

Three grt-(ky-)bearing meta-pelite samples, one from the Yuka terrane (2C123) and two from the Xitieshan terrane (Q7-24, Q7-25) were selected for zircon U–Pb SIMS dating to determine their metamorphic ages. Most zircon grains from the Yuka sample (2C123)

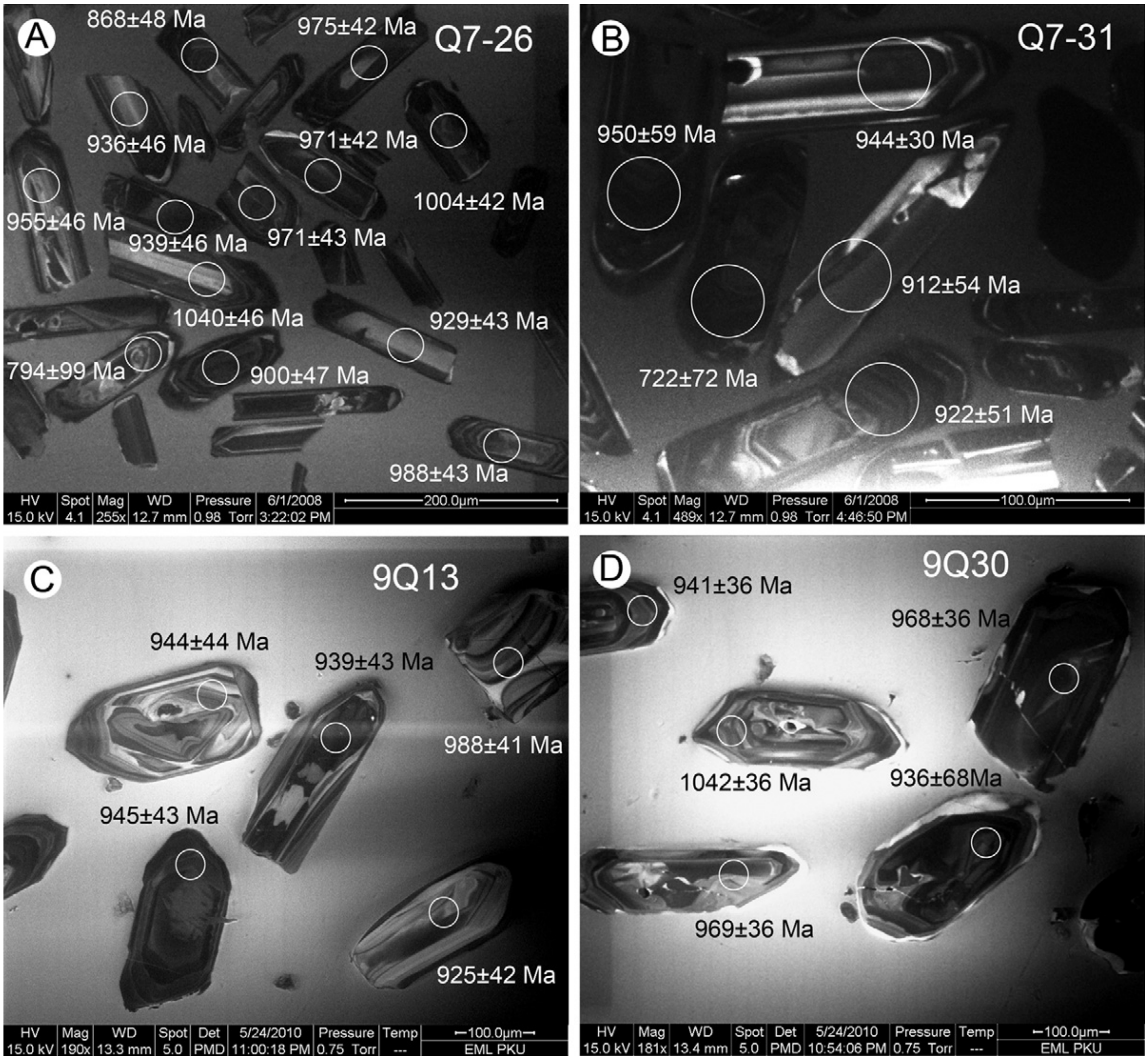

Fig. 3. Representative CL images of zircons with analytic spots and $^{207}Pb/^{206}Pb$ ages from granitic gneisses in the North Qaidam UHPM belt.

display core-rim structure in both optical and CL images; the detrital cores are mostly of magmatic origin with oscillatory bands. The rims are of metamorphic origin with Grt + Qtz inclusions (Fig. 5a) determined by Raman microspectroscopy (Ranisow RM-1000 with the 514.5 nm line of an Ar-ion laser at Peking University). CL images show planar growth banding and radial sector zoning (Fig. 5c,d) with low Th/U ratios (0.03–0.26). Some grains have very thin outer rim of bright luminescence, suggesting multiple metamorphic growth. U–Pb analyses of metamorphic rims (n = 19) give an approximately concordant population with a mean $^{207}Pb/^{206}Pb$ age of 910 ± 5 Ma (MSWD = 0.75), and eight detrital cores yield discordant ($^{207}Pb/^{206}Pb$) ages ranging from 1297 Ma to 1852 Ma.

Zircon grains recovered from two grt–ky gneiss samples (Q7-24, Q7-25) in the Xitieshan terrane are colorless and oval-shaped crystals with long axis of 50–100 μm. Garnet, quartz and kyanite (?) inclusions are also identified (Fig. 5b). CL images exhibit the type of metamorphic origin with stubby textures of "fir-tree" sector zoning, planar growth banding and radial sector zoning (Fig. 5e,f), similar to those zircons from high-grade (granulite-facies) metamorphic rocks (e.g., Vavra et al., 1996). Some zircon grains contain a small (10–20 μm) relict core with varying CL luminescence. Most zircon grains have a narrow (<10 μm), dark CL luminescent outer rim, reflecting a later thermal event associated with the determined HP–UHP metamorphism at 420–460 Ma (J.X. Zhang et al., 2008; C. Zhang et al., 2012; Song et al., 2011). U–Pb analyses for sample Q7-25 yield concordant $^{207}Pb/^{206}Pb$ ages of 899–936 Ma with a weighted mean of 916 ± 7 Ma (n = 16, MSWD = 0.71). Zircon U–Pb analyses for sample Q7-24 form a mixing line with intercepts at 928 ± 12 Ma and 421 ± 55 Ma (MSWD = 1.08) (Fig. 4b). These ages, combining UHP ages of 460–420 Ma for garnet peridotite, eclogite and metapelite published in the literatures (e.g., Song et al., 2005, 2006; Mattinson et al., 2006; J.X. Zhang et al., 2006, 2008; C. Zhang et al., 2012), suggest that metapelites in the North Qaidam UHP metamorphic belt have experienced two major epochs of metamorphism temporarily corresponding to Grenvillian and Caledonian events.

5. Discussion

5.1. Magmatism and metamorphism of Grenvillian orogeny in an active continental margin

The North Qaidam is a Caledonian-age orogenic belt of continental subduction/exhumation nature, where a great amount of continental crust was dragged down to depths of ~100–200 km and suffered HP–UHP metamorphism at ~460–420 Ma. These Neoproterozoic age of the protoliths of the UHPM rocks and host granitic gneisses, on the other hand, provide compelling evidence for the prior existence of a Grenville-age orogenic belt that had participated in the younger Caledonian-age UHPM in this region. Zircons

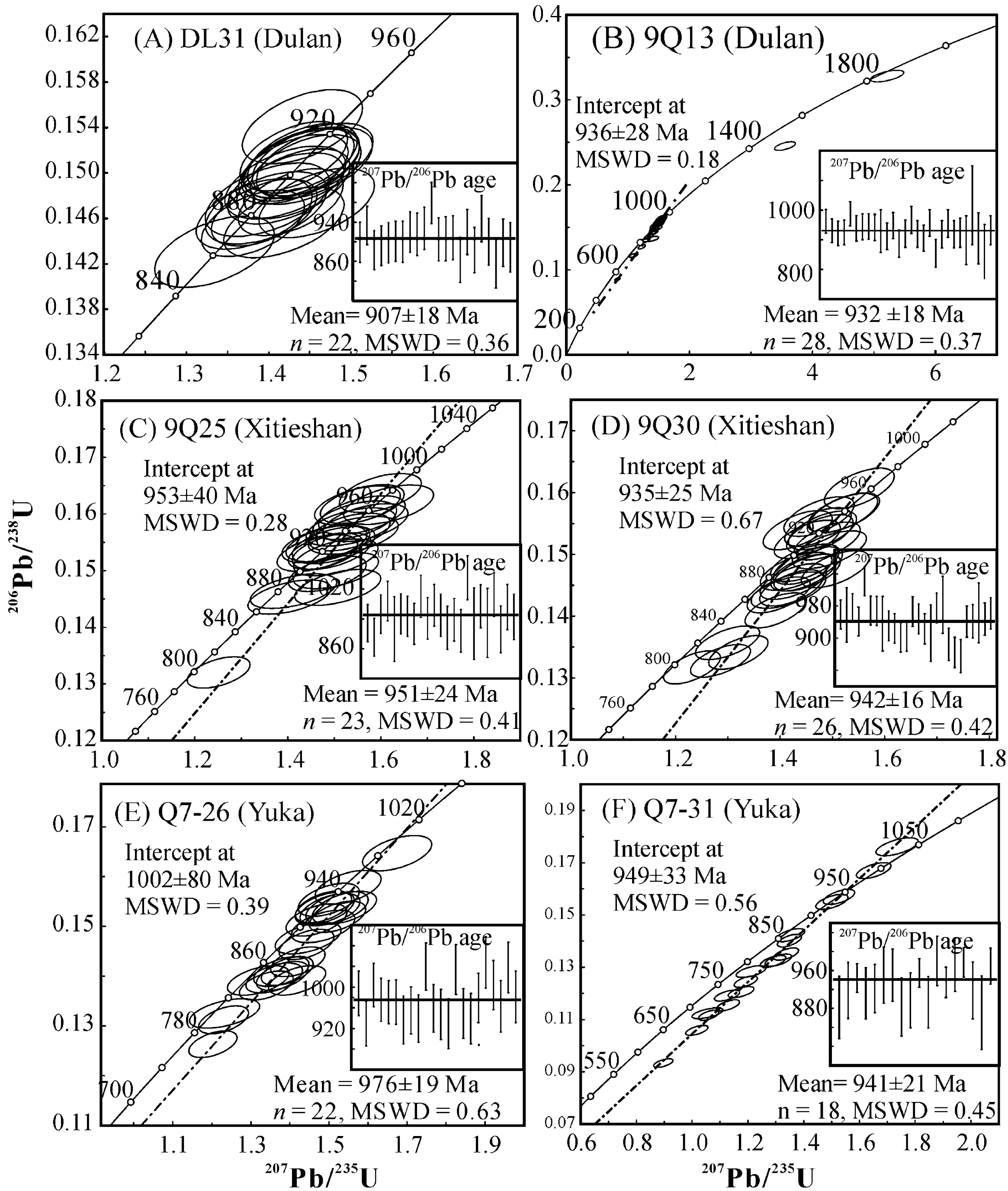

Fig. 4. Concordia diagrams showing results of individual LA-ICPMS analyses for the granitic gneiss (see sample localities in Fig. 1b).

from granitic gneisses are consistent with previous magmatic ages reported in the north part of the Qilian block (Guo et al., 1999; Lu, 2002; Wan et al., 2001; Tung et al., 2007b). Therefore, the Grenville-age magmatic activities are widespread in the Qaidam-Qilian block (Fig. 6).

Granitic gneiss of 1000–900 Ma ages is the major component (~80 vol.%) and is spatially restricted within a narrow limit along the UHPM belt, suggesting that magmatism in the Grenville-age orogenic belt is successive and most probably formed in an active continental margin. Zircons from the metapelites exhibit CL inner-structures resembling these from high-grade (granulite-facies) rocks (e.g., Vavra et al., 1996). The $^{207}Pb/^{206}Pb$ weighted mean ages from 910 ± 6 Ma to 928 ± 12 Ma, together with ~890 Ma reported by J.X. Zhang et al. (2008) and 945 ± 7 Ma by C. Zhang et al. (2003), should represent the metamorphic ages of pelitic rocks and thus are consistent with the magmatic ages. Detrital zircon cores in a the pelitic sample (2C123) give discordant $^{207}Pb/^{206}Pb$ ages ranging from 1852 to 1297 Ma, suggesting that the provenance of protoliths sediments are mainly derived from Mesoproterozoic magmatic and metamorphic rocks. Although these metapelites occur as country-rocks of the eclogite blocks and their rock-forming minerals (garnet + kyanite) may be either Grenville-age high-grade or Caledonian-age UHP metamorphism, very thin zircon rims suggest that metamorphic growth was limited during Caledonian UHP metamorphism because of relatively dry condition during continental subduction (Song et al., 2010a,b). Therefore, Grenville-age high-grade metamorphism occurred in time and space consistent with the magmatic belt. They composed an integrate

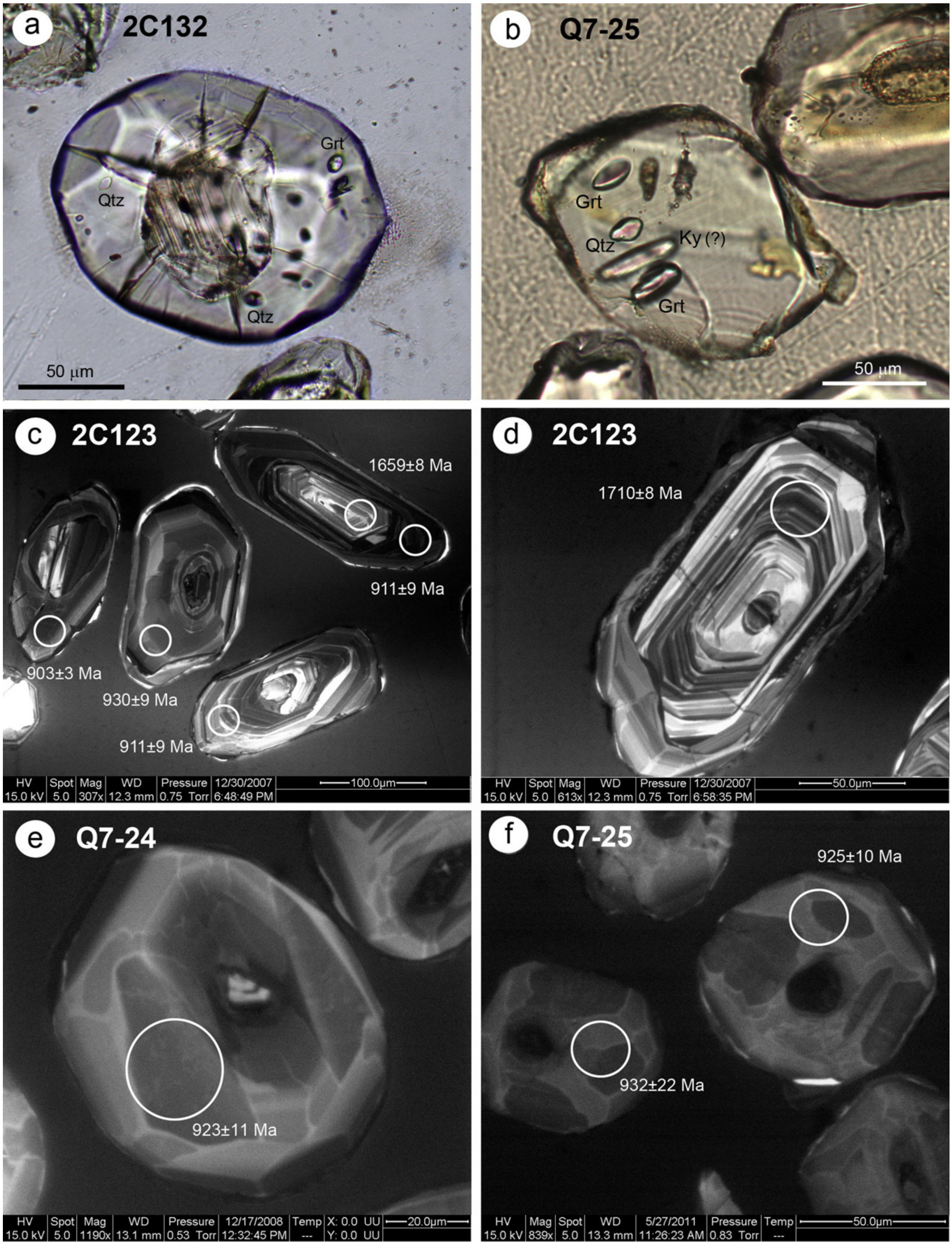

Fig. 5. Photomicrographs and CL images showing analytic spots and $^{207}Pb/^{206}Pb$ ages for zircons from pelitic gneisses.

tectono-thermal event, mostly in an environment of active continental margin in the Meso- to Neoproterozoic time.

Grenville-age orogeny is a long-lived, worldwide mountain building event that assembled the supercontinent Rodinia and has been recognized in eastern N. America, eastern Greenland, Scandinaviais, Australia, and South China (e.g., Borg and DePaolo, 1994; Fitzsimons, 2000; Li et al., 2002, 2008; Davidson, 2008). Most researchers inferred that the peak of the orogeny ranges from 1.3 Ga to 1.0 Ga in the major Grenville belts, but orogenic events between ca. 1000 and ca. 900 Ma are also found in Eastern Ghats Belt of India and East Antarctica and South China (e.g., Mezger and Cosca, 1999; Boger et al., 2000; Fitzsimons, 2000; Kelly et al., 2002; Li et al., 2006, 2009b; Z.-X. Li et al., 2008).

The coevality of magmatism and metamorphism (~1000–900 Ma) in the study area is younger than typical Grenvillian orogen in Texas and Grenville Province in southern

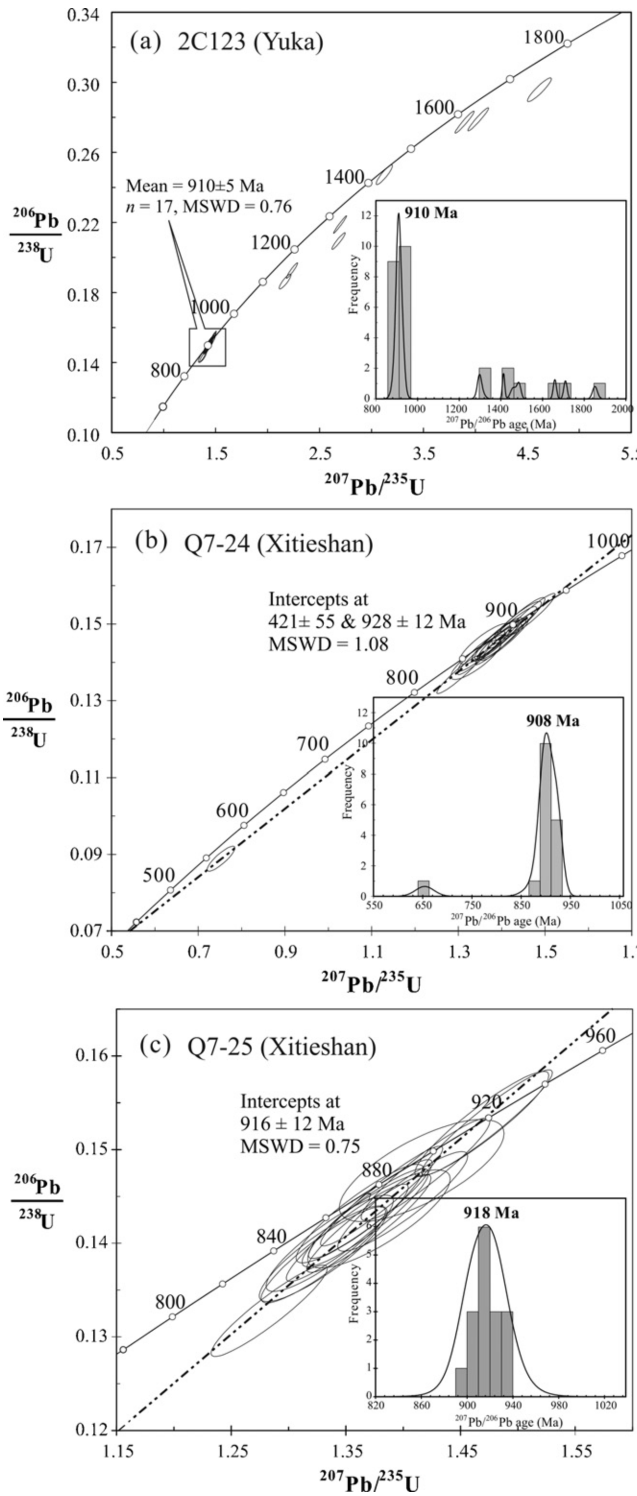

Fig. 6. Concordia and histograms of metamorphic zircons showing results of SIMS analyses for the metapelite (see sample localities in Fig. 1b).

Laurentia and Albany-Fraser and Musgrave orogeny in central Australia (1300–1050 Ma), but is temporally comparable with 950–900 Ma arc volcanism along the northern margin of the Yangtze craton (Ling et al., 2003), 863–971 Ma granitic gneisses in the Qinling orogenic belt (Lu et al., 2005), and the 990–900 Ma high-grade metamorphism in both the Eastern Ghats Belt of India and the corresponding Rayner Province in East Antarctica (Kelly et al., 2002).

5.2. The link between South China and Tarim Blocks

The SCC was thought to be formed by amalgamation between the Yangtze and Cathaysia Blocks in Grenvillian time along the Sibao (or Jiangnan) Orogen at ca. 900 Ma (e.g., Li et al., 2009b), as seen the ~1.0–0.9 Ga metamorphism, arc and back-arc magmatism along the southeastern margin of the Yangtze Block. The 1000–900 Ma magmatism also occurs in the north part of the Yangtze block; this includes (1) 950–900 Ma arc volcanic rocks (basalt–rhyolite succession) along the northern margin of the Yangtze Block (Ling et al., 2003), and (2) 970–860 Ma granitic gneisses in the Qinling Paleozoic UHPM belt (e.g., Lu et al., 2005). The 950–900 Ma arc volcanic rocks along the northern margin of Yangtze block (Ling et al., 2003) provide solid evidence for arc magmatism associated with the oceanic lithosphere subduction zone, rather than continental collision or post-collisional magmatism. The Qinling Paleozoic UHPM belt is mostly the subducted Grenville-age juvenile crust of the SCC, similar to the North Qaidam UHPM belt. Consequently, combining with the 850–750 Ma plume-related magmatism (Tseng et al., 2006; Lu, 2002; Song et al., 2010a,b; Tung et al., 2012), the SCC is temporally comparable to the Qaidam-Qilian block in terms of Grenvillian orogeny; that is, the Qaidam-Qilian block is most likely the west extension of the SCC.

The Tarim block was thought to be an individual block apart from the Yangtze block in most geological history and has been situated at different positions in previous Rodinia reconstructions (e.g., Condie, 2000; Li et al., 1996, 2002, 2008; Lu et al., 2008). Li et al. (2008) suggested that the Tarim block might join Australia on the north during the late stage of the Genvillian orogeny (ca. 900 Ma) as indicated by the ^{40}Ar–^{39}Ar cooling ages of 872–862 Ma (Zhang L.F., unpublished data, as quoted in Chen et al., 2004) from the Aksu blueschist which is intruded by 807 ± 12 Ma mafic dykes (Chen et al., 2004).

Much of the Precambrian basement of the Tarim block is little known because of the thick covers throughout the block. In Quruqtagh region of northeastern Tarim Craton, 830–750 Ma magmatism including ultramafic–mafic–carbonatite complex and granites is well-developed in the Precambrian basement (C.L. Zhang et al., 2007; Xu et al., 2005, 2009; Lu et al., 2008); some Grenvillian age data including whole-rock Sm–Nd isochron age of 1200 ± 82 Ma from a rhyolite and Ar–Ar ages of 1050 ± 1 Ma and 1021 ± 1 Ma from an amphibolite have also been reported (C.L. Zhang et al., 2003). At the east bound, the Tarim block is offset by the Altyn Tagn Fault, and the Qaidam-Qilian block in the east side of the fault was transported for ~400 km to the northeast, as indicated by corresponding HP and UHP metamorphic belts. Meanwhile, some Grenvillian age (1035–900 Ma) granitic gneisses and detrital zircon population were also reported in the Altun UHPM terrane (Gehrels and Yin, 2003; Wang et al., 2006; Qin et al., 2008; Zhang et al., 2011) (Fig. 1a). Therefore, the Tarim and Qaidam-Qilian is likely a single block before the sinistral transference of Altyn Tagn Fault in response to the India–Asia collision.

6. Summary

The ~900–1000 Ma granitic gneisses and metapelite in the North Qaidam UHPM belt indicate a Grenville-age juvenile crustal accretion and provide further evidence for the presence of the magmatic-metamorphic activity in an Andean-type active continental margin in the Meso- to Neoproterozoic. Paleozoic continental subduction brought these Grenville-age crustal rocks down to depths of 100–200 km, suggesting multi-cycle continental orogenesis along the north margin of the Qaidam-Qilian block., including Grenville-age convergence to form the supercontinent Rodinia, the afterward divergence in the Neoproterozoic, and the final re-convergence in the Early Paliozoic. The Grenville-age orogenic belt extends from the Yangtze block in the east, via Qaidam-Qilian block in the middle, and to Tarim in the west, providing a key link for the "South-West China United Continent". This continent was most likely united with the India-East Antarctica continents in Early Neoproterozoic.

Acknowledgments

This study was supported by National Natural Science Foundation of China (Grant Nos. 40825007, 40821002, 40773012), the Major State Basic Research Development Projects (2009CB825007), and Basic geological survey program of China Geological Survey (1212011121258). We thank two anonymous reviewers for their detailed and constructive review comments, which led to a better presentation of the final product.

References

Boger, S.D., Carson, C.J., Wilson, C.J.L., Fanning, C.M., 2000. Neoproterozoic deformation in the Radok Lake region of the northern Prince Charles Mountains, east Antarctica; evidence for a single protracted orogenic event. Precambrian Research 104, 1–24.

Borg, S.G., DePaolo, D.J., 1994. Laurentia, Australia, and Antarctica as a Late Proterozoic supercontinent: constraints from isotopic mapping. Geology 22, 307–310.

Chen, D.L., Liu, L., Sun, Y., Liou, J.G., 2009a. Geochemistry and zircon U–Pb dating and its implications of the Yukahe HP/UHP terrane, the North Qaidam, NW China. Journal of Asian Earth Sciences 35, 259–272.

Chen, N., Gong, S., Sun, M., Li, X., Xia, X., Wang, Q., Wu, F., Xu, P., 2009b. Precambrian evolution of the Quanji Block, northeastern margin of Tibet: insights from zircon U–Pb and Lu–Hf isotope compositions. Journal of Asian Earth Sciences 35, 367–376.

Chen, N.S., Wang, Q.Y., Chen, Q., Li, X.Y., 2007. Components and metamorphism of the basements of the Qaidam and Oulongbuluke micro-continental blocks, and a tentative interpretation of paleocontinental evolution in NW-Central China. Earth Science Frontiers 14, 43–55 (in Chinese with English abstract).

Chen, Y., Xu, B., Zhan, S., Li, Y.G., 2004. First mid-Neoproterozoic paleomagnetic results from the Tarim Basin (NW China) and their geodynamic implications. Precambrian Research 133, 271–281.

Condie, K.C., 2000. Episodic continental growth models: afterthoughts and extensions. Tectonophysics 322, 153–162.

Davidson, A., 2008. Late Paleoproterozoic to mid-Neoproterozoic history of northern Laurentia: an overview of central Rodinia. Precambrian Research 160, 5–22.

Dan, W., Li, X.-H., Guo, J., Liu, Y., Wang, X.-C., 2012. Paleoproterozoic evolution of the eastern Alxa Block, westernmost North China: evidence from in situ zircon U–Pb dating and Hf–O isotopes. Gondwana Research 21, 838–864.

Fitzsimons, I.C.W., 2000. Grenville-age basement provinces in East Antarctica: evidence for three separate collisional orogens. Geology 28, 879–882.

Gehrels, G.E., Yin, A., 2003. Magmatic history of the northeastern Tibetan Plateau. Journal of Geophysical Research 108 (B9), 2423.

Geng, Y.-S., Wang, X.S., Shen, Q.H., Wu, C.M., 2006. Redefinition of the Alxa Group-complex (Precambrian metamorphic basement) in the Alxa area, Inner Mongolia. Geology in China 33, 138–145 (in Chinese with English abstract).

Geng, Y.S., Wang, X.S., Shen, Q.H., Wu, C.M., 2007. Chronology of the Precambrian metamorphic series in the Alxa area, Inner Mongolia. Geology in China 34, 251–261 (in Chinese with English abstract).

Guo, J.J., Zhao, F.Q., Li, H.K., 1999. Jinningian Collisional Granite Belt in the Eastern sector of the Central Qilian Massif and its implication. Acta Geoscientia Sinica 20, 10–15 (in Chinese with English abstract).

Hacker, B.R., Ratschbacher, L., Webb, L.E., Ireland, T., Walker, D., Dong, S., 1998. Zircon ages constrain the architecture of the ultrahigh-pressure Qinling-Dabie orogen, China. Earth and Planetary Science Letters 161, 215–230.

Kelly, N.M., Clarke, G.L., Fanning, C.M., 2002. A two-stage evolution of the Neoproterozoic Rayner Structural Episode: new U–Pb sensitive high resolution ion microprobe constraints from the Oygarden Group, Kemp Land, East Antarctica. Precambrian Research 116, 307–330.

Li, Q.L., Li, X.H., Liu, Y., Tang, G.Q., Yang, J.H., Zhu, W.G., 2010. Precise U–Pb and Pb–Pb dating of Phanerozoic baddeleyite by SIMS with oxygen flooding technique. Journal of Analytical Atomic Spectrometry 25, 1107–1113.

Li, S., Xiao, Y., Liou, D., Chen, Y., Ge, N., Zhang, Z., Sun, S.-S., Cong, B., Zhang, R., Hart, S.R., Wang, S., 1993. Collision of the North China and Yangtze blocks and formation of coesite-bearing eclogites: timing and processes. Chemical Geology 109, 89–111.

Li, X.-H., Su, L., Chung, S.L., Li, Z.X., Liu, Y., Song, B., Liu, D.Y., 2005. Formation of the Jinchuan ultramafic intrusion and the world's third largest Ni–Cu sulfide deposit: associated with the ~825 Ma south China mantle plume? Geochemistry, Geophysics, Geosystems 6, Q11004.

Li, X.-H., Li, Z.-X., Sinclair, J.A., Li, W.-X., Carter, G., 2006. Revisiting the "Yanbian Terrane": implications for Neoproterozoic tectonic evolution of the western Yangtze Block, South China. Precambrian Research 151, 14–30.

Li, X.-H., Li, W.-X., Li, Z.-X., Lo, C.-H., Wang, J., Ye, M.-F., Yang, Y.-H., 2009a. Amalgamation between the Yangtze and Cathaysia Blocks in South China: constraints from SHRIMP U–Pb zircon ages, geochemistry and Nd–Hf isotopes of the Shuangxiwu volcanic rocks. Precambrian Research 174, 117–128.

Li, X.-H., Liu, Y., Li, Q.L., Guo, C.H., Chamberlain, K.R., 2009b. Precise determination of Phanerozoic zircon Pb/Pb age by multicollector SIMS without external standardization. Geochemistry, Geophysics, Geosystems 10, Q04010, http://dx.doi.org/10.1029/2009GC002400.

Li, Z.X., Zhang, L., Powell, C.M., 1996. Positions of the East Asian cratons in the Neoproterozoic supercontinent Rodinia. Australian Journal of Earth Science 43, 593–604.

Li, Z.-X., Li, X.-h., Zhou, H., Kinny, P.D., 2002. Grenvillian continental collision in south China: new SHRIMP U–Pb zircon results and implications for the configuration of Rodinia. Geology 30, 163–166.

Li, Z.-X., Bogdanova, S.V., Collins, A.S., Davidson, A., De Waele, B., Ernst, R.E., Fitzsimons, I.C.W., Fuck, R.A., Gladkochub, D.P., Jacobs, J., Karlstrom, K.E., Lu, S., Natapov, L.M., Pease, V., Pisarevsky, S.A., Thrane, K., Vernikovsky, V., 2008. Assembly, configuration, and break-up history of Rodinia: a synthesis. Precambrian Research 160, 179–210.

Ling, W., Gao, S., Zhang, B., Li, H., Liu, Y., Cheng, J., 2003. Neoproterozoic tectonic evolution of the northwestern Yangtze craton, South China: implications for amalgamation and break-up of the Rodinia Supercontinent. Precambrian Research 122, 111–140.

Lu, S.N., 2002. Preliminary Study of Precambrian Geology in the North Tibet-Qinghai Plateau. Geological Publishing House, Beijing, 125 pp. (in Chinese).

Lu, S.N., Chen, Z.H., Li, H.K., Hao, G.J., 2005. Two magmatic belts of the Neoproterozoic in the Qinling orogenic belt. Acta Geologica Sinica 79, 165–173.

Lu, S.N., Yu, H.F., Li, H.K., 2006. Research on Precambrian Major Problems in China. Geological Publishing House, pp. 1–206 (in Chinese).

Lu, S.N., Li, H.K., Zhang, C.L., Niu, G.H., 2008. Geological and geochronological evidence for the Precambrian evolution of the Tarim Craton and surrounding continental fragments. Precambrian Research 160, 94–107.

Mattinson, C.G., Wooden, J.L., Liou, J.G., Bird, D.K., Wu, C.L., 2006. Age and duration of eclogite-facies metamorphism, North Qaidam HP/UHP terrane, western China. American Journal of Science 306, 683–711.

Mattinson, C.G., Wooden, J.L., Zhang, J.X., Bird, D.K., 2009. Paragneiss zircon geochronology and trace element geochemistry, North Qaidam HP/UHP terrane, western China. Journal of Asian Earth Sciences 35, 298–309.

Menold, C.A., Manning, C.E., Yin, A., Tropper, P., Chen, X.H., Wang, X.F., 2009. Metamorphic evolution, mineral chemistry and thermobarometry of orthogneiss hosting ultrahigh-pressure eclogites in the North Qaidam metamorphic belt, Western China. Journal of Asian Earth Sciences 35, 273–284.

Mezger, K., Cosca, M.A., 1999. The thermal history of the Eastern Ghats Belt (India) as revealed by U–Pb and $^{40}Ar/^{39}Ar$ dating of metamorphic and magmatic minerals; implications for the SWEAT correlation. Precambrian Research 94, 251–271.

Qin, X.F., Xia, B., Li, C.Q., Li, J., Lu, J.P., Xu, H., Zhou, F.S., Hu, G., Li, Q., 2008. Geochemical characteristics and tectonic setting of Precambrian granitic gneiss in the western segment of Altyn Tagh tectonic belt. Geoscience 22, 34–44.

Replumaz, A., Tapponnier, P., 2003. Reconstruction of the deformed collision zone Between India and Asia by backward motion of lithospheric blocks. Journal of Geophysical Research 108 (B6), 2285, http://dx.doi.org/10.1029/2001JB000661.

Song, S.G., Yang, J.S., Xu, Z.Q., Liou, J.G., Shi, R.D., 2003. Metamorphic evolution of the coesite-bearing ultrahigh-pressure terrane in the North Qaidam, Northern Tibet, NW China. Journal of Metamorphic Geology 21, 631–644.

Song, S.G., Zhang, L.F., Niu, Y.L., Su, L., Jian, P., Liu, D.Y., 2005. Geochronology of diamond-bearing zircons from garnet peridotite in the North Qaidam UHPM belt, Northern Tibetan Plateau: a record of complex histories from oceanic lithosphere subduction to continental collision. Earth and Planetary Science Letters 234, 99–118.

Song, S.G., Zhang, L.F., Niu, Y.L., Su, L., Song, B.A., Liu, D.Y., 2006. Evolution from oceanic subduction to continental collision: a case study from the Northern Tibetan Plateau based on geochemical and geochronological data. Journal of Petrology 47, 435–455.

Song, S.G., Zhang, L.F., Niu, Y.L., Wie, C.J., Liou, J.G., Shu, G.M., 2007. Eclogite and carpholite-bearing metasedimentary rocks in the North Qilian suture zone, NW China: implications for early palaeozoic cold oceanic subduction and water transport into mantle. Journal of Metamorphic Geology 25, 547–563.

Song, S.G., Niu, Y.L., Zhang, L.F., Wei, C.J., Liou, J.G., Su, L., 2009. Tectonic evolution of early Paleozoic HP metamorphic rocks in the North Qilian Mountains, NW China: new perspectives. Journal of Asian Earth Sciences 35, 334–353.

Song, S.G., Su, L., Li, X.H., Zhang, G.B., Niu, Y.L., Zhang, L.F., 2010a. Tracing the 850-Ma continental flood basalts from a piece of subducted continental crust in the North Qaidam UHPM belt, NW China. Precambrian Research 183, 805–816.

Song, S.G., Niu, Y.L., Wei, C.J., Ji, J.Q., Su, L., 2010b. Metamorphism, anatexis, zircon ages and tectonic evolution of the Gongshan block in the northern Indochina continent – an eastern extension of the Lhasa Block. Lithos 120, 327–346.

Song, S.G., Zhang, C., Li, X.H., 2011. HP/UHP metamorphic time of eclogite in the Xitieshan terrane, North Qaidam UHPM belt, NW China. Acta Petrologica Sinica 27 (4), 1191–1197.

Song, S.G., Niu, Y.L., Su, L., 2012. Tectonics of the North Qilian orogen, NW China. Gondwana Research, http://dx.doi.org/10.1016/j.gr.2012.02.004.

Stacey, J.S., Kramers, J.D., 1975. Approximation of terrestrial lead isotope evolution by a two-stage model. Earth and Planetary Science Letters 26, 207–221.

Tapponnier, P., Xu, Z.Q., Roger, F., Meyer, B., Arnaud, N., Wittlinger, G., Yang, J.S., 2001. Oblique stepwise rise and growth of the Tibet plateau. Science 294, 1671–1677.

Tian, W., Campbell, I., Allen, C., Guan, P., Pan, W., Chen, M., Yu, H., Zhu, W., 2010. The Tarim picrite–basalt–rhyolite suite, a Permian flood basalt from northwest China with contrasting rhyolites produced by fractional crystallization and anatexis. Contributions to Mineralogy and Petrology 160, 407–425.

Tseng, C.Y., Yang, H.Y., Wan, Y.S., Liu, D.Y., Wen, D.J., Lin, T.C., Tung, K.A., 2006. Finding of Neoproterozoic (~775 Ma) magmatism recorded in metamorphic complexes from the North Qilian orogen: evidence from SHRIMP zircon U–Pb dating. Chinese Science Bulletin 51, 963–970.

Tung, K.A., Yang, H.Y., Liu, D.Y., Zhang, J.X., Tseng, C.Y., Wan, Y.S., 2007a. SHRIMP U–Pb geochronology of the detrital zircons from the Longshoushan group and its tectonic significance. Chinese Science Bulletin 52, 1414–1425.

Tung, K.A., Yang, H.J., Yang, H.Y., Liu, D.Y., Zhang, J.X., Wan, Y.S., Tseng, C.Y., 2007b. SHRIMP U–Pb geochronology of the zircons from the Precambrian basement of the Qilian Block and its geological significances. Chinese Science Bulletin 52, 2687–2701.

Tung, K.-A., et al., 2012. The amphibolite-facies metamorphosed mafic rocks from the Maxianshan area, Qilian block, NW China: a record of early Neoproterozoic arc magmatism. Journal of Asian Earth Sciences, http://dx.doi.org/10.1016/j.jseaes.2011.12.006.

Vavra, G., Gebauer, D., Schmidt, R., Compston, W., 1996. Multiple zircon growth and recrystallization during polyphase Late Carboniferous to Triassic metamorphism in granulites of the Ivrea Zone (Southern Alps): an ion microprobe (SHRIMP) study. Contributions to Mineralogy and Petrology 122, 337–358.

Wan, Y.S., Xu, Z.Q., Yan, J.S., Zhang, J.X., 2001. Ages and compositions of the Precambrian high-grade basement of the Qilian Terrane and its adjacent areas. Acta Geologica Sinica 75, 375–384.

Wan, Y.S., Zhang, J.X., Yang, J.S., Xu, Z.Q., 2006. Geochemistry of high-grade metamorphic rocks of the North Qaidam Mountains and their geological significance. Journal of Asian Earth Sciences 28, 174–184.

Wang, C., Liu, L., Che, Z.C., Chen, D.L., Zhang, A.D., Luo, J.H., 2006. U–Pb geochronology and tectonic setting of the granitic gneiss in Jianggaleisayi eclogite belt, the southern edge of Altyn Tagh. Geological Journal of China Universities 12, 74–82.

Wang, Q.Y., Pan, Y.M., Chen, N.S., Li, X.Y., Chen, H.H., 2009. Proterozoic polymetamorphism in the Quanji Block, northwestern China: evidence from microtextures, garnet compositions and monazite CHIME ages. Journal of Asian Earth Sciences 34, 686–698.

Wiedenbeck, M., Alle, P., Corfu, F., Griffin, W.L., Meier, M., Oberli, F., Vonquadt, A., Roddick, J.C., Speigel, W., 1995. Three natural zircon standards for U–Th–Pb, Lu–Hf, trace-element and REE analyses. Geostandard Newsletters 19, 1–23.

Wu, H.Q., Feng, Y.M., Song, S.G., 1993. Metamorphism and deformation of blueschist belts and their tectonic implications, North Qilian mountains, China. Journal of Metamorphic Geology 11, 523–536.

Xiu, Q.Y., Yu, H.F., Li, Q., Zuo, G.C., Li, J.W., Cao, C.J., 2004. Discussion on the petrogenic time of Longshoushan Group, Gansu Province. Acta Geologica Sinica 78, 366–373.

Xu, B., Jian, P., Zheng, H., Zou, H., Zhang, L., Liu, D., 2005. U–Pb zircon geochronology and geochemistry of Neoproterozoic volcanic rocks in the Tarim Block of northwest China: implications for the breakup of Rodinia supercontinent and Neoproterozoic glaciations. Precambrian Research 136, 107–123.

Xu, B., Xiao, S., Zou, H., Chen, Y., Li, Z.-X., Song, B., Liu, D., Zhou, C., Yuan, X., 2009. SHRIMP zircon U–Pb age constraints on Neoproterozoic Quruqtagh diamictites in NW China. Precambrian Research 168, 247–258.

Xu, W.C., Zhang, H.F., Liu, X.M., 2007. U–Pb zircon dating constraints on formation time of Qilian high-grade metamorphic rock and its tectonic implications. Chinese Science Bulletin 52, 531–538.

Yang, J.S., Xu, Z.Q., Zhang, J.X., Song, S.G., Wu, C.L., Shi, R.D., Li, H.B., Brunel, M., 2002. Early Palaeozoic North Qaidam UHP metamorphic belt on the north-eastern Tibetan plateau and a paired subduction model. Terra Nova 14 (5), 397–404.

Ye, M.-F., Li, X.-H., Li, W.-X., Liu, Y., Li, Z.-X., 2007. SHRIMP zircon U–Pb geochronological and whole-rock geochemical evidence for an early Neoproterozoic Sibaoan magmatic arc along the southeastern margin of the Yangtze Block. Gondwana Research 12, 144–156.

Zhang, C.L., Dong, Y.G., Zhao, Y., Wang, A.G., 2003. Geochemistry of Mesoproterozoic volcanics in West Kunlun: evidence for plate tectonic evolution. Acta Geologica Sinica 78, 532–542.

Zhang, C., Van Roermond, H., Zhang, L.F., Spiers, C., 2012. A polyphase metamorphic evolution for the Xitieshan paragneiss of the north Qaidam UHP metamorphic belt, western China: in situ EMP monazite- and U–Pb zircon SHRIMP dating. Lithos, http://dx.doi.org/10.1016/j.lithos.2011.07.024.

Zhang, C.L., Li, X.-H., Li, Z.-X., Lu, S.N., Ye, H.M., Li, H.M., 2007a. Neoproterozoic ultramafic–mafic–carbonatite complex and granitoids in Quruqtagh of northeastern Tarim Block, western China: geochronology, geochemistry and tectonic implications. Precambrian Research 152, 149–169.

Zhang, G.B., Song, S.G., Zhang, L.F., Niu, Y.L., 2008a. The subducted oceanic crust within continental-type UHP metamorphic belt in the North Qaidam NW China: evidence from petrology, geochemistry and geochronology. Lithos 104, 99–108.

Zhang, J.X., Wan, Y.S., Xu, Z.Q., Yang, J.S., Meng, F.C., 2001a. Discovery of basic granulite and its formation age in Delingha area, North Qaidam Mountains. Acta Petrologica Sinica 17, 453–458 (in Chinese with English abstract).

Zhang, J.X., Zhang, Z.M., Xu, Z.Q., Yang, J.S., Cui, J.W., 2001b. Petrology and geochronology of eclogites from the western segment of the Altyn Tagh, Northwestern China. Lithos 56, 187–206.

Zhang, J.X., Yang, J.S., Meng, F.C., Wan, Y.S., Li, H., Wu, C.L., 2006. U–Pb isotopic studies of eclogites and their host gneisses in the Xitieshan area of the North Qaidam mountains, western China: new evidence for an early Paleozoic HP–UHP metamorphic belt. Journal of Asian Earth Sciences 28, 143–150.

Zhang, J.X., Meng, F.C., Wan, Y.S., 2007b. A cold Early Palaeozoic subduction zone in the North Qilian Mountains, NW China: petrological and U–Pb geochronological constraints. Journal of Metamorphic Geology 25, 285–304.

Zhang, J.X., Mattinson, C.G., Meng, F.C., Wan, Y.S., Tung, K., 2008b. Polyphase tectonothermal history recorded in granulitized gneisses from the North Qaidam HP/UHP metamorphic terrane, Western China: evidence from zircon U–Pb geochronology. Geological Society of America Bulletin 120, 732–749.

Zhang, J.X., Li, H.K., Meng, F.C., Xiang, Z.Q., Yu, S.Y., Li, J.P., 2011. Polyphase tectonothermal events recorded in "metamorphic basement" from the Altyn Tagh, the southeastern margin of the Tarim basin, western China: constraint from U–Pb zircon geochronology. Acta Petrologica Sinica 27, 23–46.

Zhang, J.X., Mattinson, C.G., Yu, S.Y., Li, J.P., Meng, F.C., 2010. U–Pb zircon geochronology of coesite-bearing eclogites from the southern Dulan area of the North Qaidam UHP terrane, northwestern China: spatially and temporally extensive UHP metamorphism during continental subduction. Journal of Metamorphic Geology 28, 955–978.

Zhao, G.C., Sun, M., Wilde, S.A., Li, S.Z., 2005. Late Archean to Paleoproterozoic evolution of the North China Craton: key issues revisited. Precambrian Research 136, 177–202.